

Effective String Rope Model for the initial stages of Ultra-Relativistic Heavy Ion Collisions

V.K. Magas^{a,b} L.P. Csernai^{b,c} D. Strottman^d

^a *Center for Physics of Fundamental Interactions, Department of Physics
Instituto Superior Tecnico, Av. Rovisco Pais, 1049-001 Lisbon, Portugal*

^b *Section for Theoretical and Computational Physics, Department of Physics
University of Bergen, Allegaten 55, N-5007, Norway*

^c *KFKI Research Institute for Particle and Nuclear Physics
P.O.Box 49, 1525 Budapest, Hungary*

^d *Theoretical Division, Los Alamos National Laboratory
Los Alamos, NM, 87454, USA*

Abstract

Different approaches to describe initial stages of relativistic heavy ion collisions are discussed qualitatively and quantitatively. An Effective String Rope Model is presented for heavy ion collisions at RHIC energies. Our model takes into account baryon recoil for both target and projectile, arising from the acceleration of partons in an effective field, $F^{\mu\nu}$, produced in the collision. The typical field strength (string tension) for RHIC energies is about $5 - 12 \text{ GeV}/\text{fm}$, what allows us to talk about “string ropes”. The results show that a QGP forms a tilted disk, such that the direction of the largest pressure gradient stays in the reaction plane, but deviates from both the beam and the usual transverse flow directions. The produced initial state can be used as an initial condition for further hydrodynamical calculations. Such initial conditions lead to the creation of third flow component.

Key words: ultra-relativistic heavy ion collisions, initial state, string ropes, RHIC, third flow

PACS: 25.75.-q, 24.85.+p, 25.75.Ld, 24.10.Jv

Email addresses: vladimir@cfif.ist.utl.pt (V.K. Magas),
csernai@fi.uib.no (L.P. Csernai), dds@lanl.gov (D. Strottman).

1 Introduction

Fluid dynamical models are widely used to describe heavy ion collisions. Their advantage is that one can vary flexibly the Equation of State (EoS) of the matter and test its consequences on the reaction dynamics and the outcome. This makes fluid dynamical models a very powerful tool to study possible phase transitions in heavy ion collisions - such as the liquid-gas or the Quark-Gluon Plasma (QGP) phase transition. For example, the only models that can handle the supercooled QGP are hydrodynamical models with a corresponding EoS. For highest energies achieved nowadays at RHIC hydrodynamic calculations give a good description of the observed radial and elliptic flows [1–6], in contrast to microscopic models, like HIJING [7] and UrQMD [8].

In energetic collisions of large heavy ions, especially if a QGP is formed in the collision, one-fluid dynamics is a valid and good description for the intermediate stages of the reaction. Here, interactions are strong and frequent, so that other models, (e.g. transport models, string models, etc., that assume binary collisions, with free propagation of constituents between collisions) have limited validity. On the other hand, the initial and final, Freeze Out (FO), stages of the reaction are outside the domain of applicability of the fluid dynamical model.

Thus, the realistic, and detailed description of an energetic heavy ion reaction requires a Multi Module Model, where the different stages of the reaction are each described with a suitable theoretical approach. It is important that these Modules are coupled to each other correctly: on the interface, which is a three dimensional hypersurface in space-time with normal $d\sigma^\mu$, all conservation laws should be satisfied, and entropy should not decrease. These matching conditions were worked out and studied for the matching at FO hypersurfaces in details in Refs. [9–11]. In Ref [12] it has been shown that the entropy constraint is very sensitive to the pre-FO EoS, i.e. the arbitrary choice of the pre-FO state does not necessarily lead to the physical FO.

Similar ideas form the base of Ref. [13,6,14] where authors combined two modules - hydro and UrQMD - replacing the hadronic phase of hydrodynamics with hadronic transport model to describe properly chemical and thermal FO.

The initial stages are the most problematic. We will discuss here different models for the initial state in section 2 and will present our modeling of it in section 3.

Our goal is to build a Multi Module Model for ultra-relativistic heavy ion collisions that is valid for RHIC and LHC energies, and maybe for the most energetic SPS collisions. The present work is just the first step, but an important one: the Effective String Rope model is developed for the most problematic

module - module describing the initial stages of collisions.

2 Initial state of Relativistic Heavy Ion Collision

The situation at the beginning of an energetic heavy ion collision is highly complicated and not easily understandable. None of the theoretical models currently on the physics market can unambiguously describe the initial stages.

As was pointed out in the introduction, at ultra-relativistic energies the one-fluid dynamical models can not be justified for such a situation. Frequently, two- or three-fluid models are used to remedy the difficulties and to model the process of QGP formation and thermalization [15–17]. Here the problem is transferred to the determination of drag-, friction- and transfer- terms among the fluid components, and a new problem is introduced with the (unjustified) use of an EoS in each component in a nonequilibrated situation where an EoS is not defined. Strictly speaking this approach can only be justified for mixtures of noninteracting ideal gas components.

The kinetic transport models (see for example, Ultra-relativistic Quantum Molecular Dynamics (UrQMD) [18]) and parton cascades (see for example, the Molnar Parton Cascade (MPC) [19,20]) are also frequently applied to describe the high energy collisions from the very beginning. Some of the parton cascades (for example, MPC) are able to handle only $2 \rightarrow 2$ reactions so far, what cannot be justified for dense and strongly interacting systems. The parton cascades also have to approximate media-effects, since the parton structure function, measured for a free nucleon, is modified inside the nucleus. This is the so-called shadowing effect [21]. This approximation procedure is also not unambiguous, see for example Ref. [22,23] for more details.

Some models, like UrQMD, were initially developed for much lower energies than available nowadays, but even then, when the particle propagates in a hot and dense and nonequilibrated medium of highly excited hadrons, the properties of this particle might change significantly. Thus, properties like effective masses, decay widths, effective momenta, and in-medium cross sections have to be calculated for a given local situation at the point where particle propagates. Unfortunately this is a very complicated and numerically very time consuming task, so in most of the models drastic approximations are made (see for example [18]). In a relativistic heavy ion collision, especially at the early stages, the excitation energy per particle would be so high that the concept of resonance (we have to deal not only with nucleons, but with many different baryons and mesons) has no sense any more. Here the quark and gluon degrees of freedom must be taken into account. Therefore, some models, including UrQMD, replace the resonances by continuous string exci-

tations for internal excitation energies higher than approximately 2 GeV . The properties of such effective “strings” are basically unknown and can be varied within a wide range, almost like free parameters [24].

Perturbative Quantum Chromo Dynamics (pQCD) would be, in principle, the proper model for describing our systems at very high energies. Unfortunately, pQCD itself is not applicable for heavy ion reactions at RHIC energies. Nevertheless, the pQCD calculations with some extra non-perturbative, phenomenological assumptions, like saturation of a gluon plasma, can be performed. Different models following this scenario have been proposed in [25–30]. The extension of the pQCD+saturation model for nonzero impact parameters, which is of primary interest for us, leads to serious complications in calculations [29].

Thus, since we can not unambiguously describe the initial stages of relativistic heavy ion collisions in microscopical models, we have to use some phenomenological models (in fact all the microscopical models discussed above already have some phenomenological elements).

2.1 Different models

There are two phenomenological models, which are most frequently discussed in the literature, and which claim to give us at least a qualitative understanding of the initial stages of the relativistic heavy ion collisions.

2.2 The Landau model

The Landau model has been developed to generalize the fluid dynamical approach to the energy range where we can not neglect relativistic effects, such as Lorentz contraction of the colliding nuclei. Actually the model was originally developed for pp collisions, but the generalization for AA is rather straightforward and the fluid dynamical expansion is even more justified for bigger systems.

It is the most appropriate model for relativistic heavy ion collisions in the energy range $E_{lab} = 10 - 100 A \cdot \text{GeV}$. For energies above $\gamma^{CM} \approx 3 - 10$, so in the Center of Mass (CM) frame the colliding nuclei are considerably contracted and have disk-like shapes. The Landau fluid dynamical model assumes the initial thermalized state as a static, completely stopped, homogeneous disk, contracted in the beam direction by the factor γ_{CM} (see Fig. 1). The fluid dynamical expansion initially starts in the direction of the largest pressure gradient - in the beam direction in our case. Only when the system has ex-

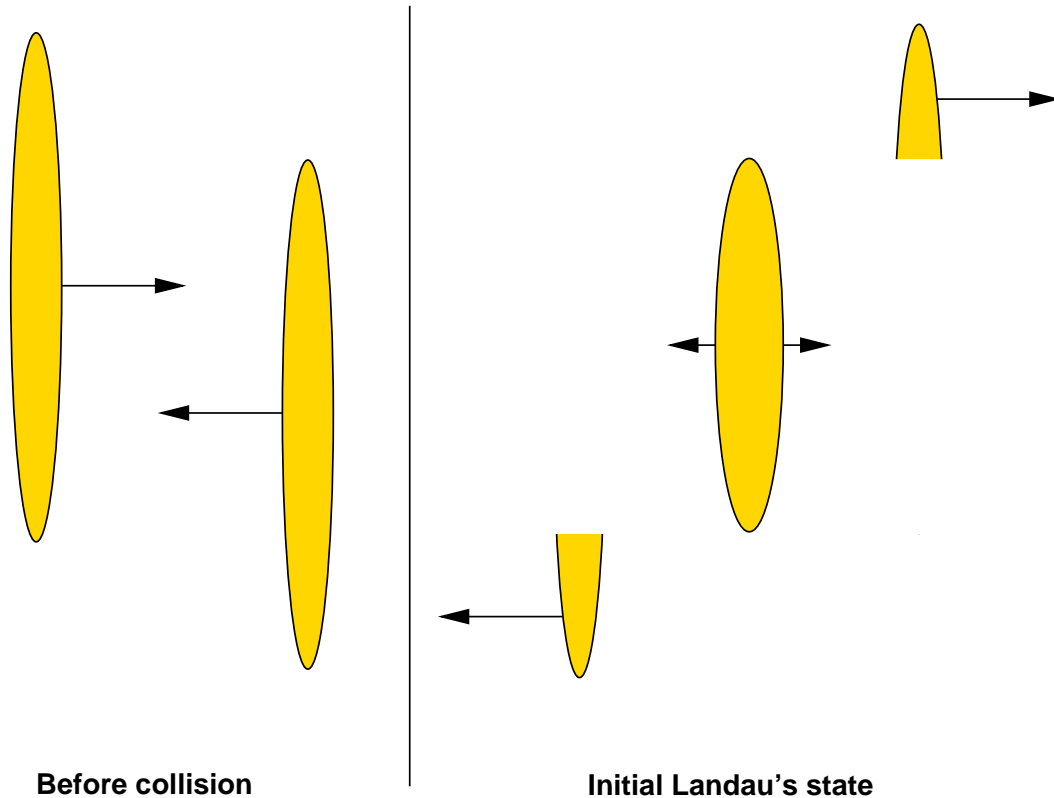


Fig. 1. Initial state in Landau model.

panded in the z direction to a size comparable to its transverse diameter the transverse expansion also considered. In this second phase the expansion is 2+1 dimensional, while initially it was 1+1 dimensional (all quantities were z and t dependent).

The inputs to this model are: A) the equation of state; B) the initial energy and baryon densities; C) the FO conditions. Usually the initial energy density, e_0 , is estimated in the following way:

$$e_0 = E_{CM}/V_0, \quad \text{where} \quad V_0 = V_{rest}/\gamma_{CM}. \quad (1)$$

2.3 The Bjorken model

If we increase the collision energy further to $E_{CM} = 100 A \cdot GeV$ or more, the expectation is that the concept of complete stopping does not work anymore. Furthermore, when two nucleons from the target and the projectile nuclei collide at these energies, their momenta are so high that they see each other as compound objects, containing three valence quarks and other partons. The point is that the proper participants at these energies are the partons and not the nucleons. The initial momenta of partons are very high and we expect these two parton clouds to cross each other and keep going with almost their original

relativistic pp collisions. The rapidity distribution of the charged particle multiplicity, dN_{ch}/dy , can be divided, with reasonable accuracy, into three regions. Two smooth peaks around $y = \pm y_0$, where y_0 is the original rapidity, are believed to be originated by target and projectile partons, interpenetrating through each other almost without rapidity lost. Between those we can see the plateau, $-dN_{ch}/dy = const$, - generated by our baryon free flux tube. Assuming the same symmetry, $dQ/dy = const$, for all other quantities a simple hydrodynamical model with an analytical solution has been developed by Bjorken in Ref. [31]. The above assumption, $dQ/dy = const$, means that our model is boost invariant - all the quantities are functions of the proper time only, $Q = Q(\tau)$, where $\tau = \sqrt{t^2 - z^2}$. Obviously the model has a 1+1 dimensional structure.

In order to study transverse expansions, the Bjorken model has to be supplemented with a description of this process separately, see for example [32]. The boost invariance of the model is also very much appreciated by theoreticians, since it is then sufficient to perform simulations for the $y = 0$ ($z = 0$) plane only, and then boost the result to reproduce all of the phase space. The Bjorken model does not tell us anything about the energy density distribution in the plane perpendicular to the beam direction, say the $z = 0$ ($y = 0$) plane; therefore additional assumptions are required. If we define a grid in the $[x, y]$ plane, then the energy density profiles proportional to the number of binary collisions, $e(x_i, y_j, z = 0) \propto N_{target}(x_i, y_j) \cdot N_{target}(x_i, y_j)$, or proportional to number of participants, $e(x_i, y_j, z = 0) \propto (N_{target}(x_i, y_j) + N_{target}(x_i, y_j))$, are the most popular assumptions in literature (see [33] for recent overview).

The initial energy density in the Bjorken model can be estimated in the following way. At the $y = 0$ ($z = 0$) plane the full energy is the transverse energy, $E_{full} = E_T$. One may also notice that for the Bjorken boost invariant model, the pseudo-rapidity ($\eta = -\ln \tan \frac{\theta}{2}$), where θ is a polar angle of emitted particle, is the same as rapidity, $\eta = y$. If in the experiment we measure the energy ΔE_T emitted in a very small rapidity window, $[0, \Delta y]$, then we can estimate the initial energy density:

$$e_0 = \frac{\Delta E_{full}}{\Delta V} = \left(\frac{\Delta E_T}{A \Delta z} \right)_{y=0} .$$

Now using the following expressions: transverse area $A = \pi R_A^2$, where R_A is the radius of nucleus with A nucleons, and size in the beam direction $\Delta z = \tau \Delta \eta = \tau_0 \Delta y$, where τ_0 is the thermalization time, - we obtain

$$e_0 = \frac{1}{\pi R_A^2 \tau_0} \left(\frac{dE_T}{dy} \right)_{y=0} . \quad (2)$$

Here the thermalization time is unknown and should be estimated from some

other model for the particular reaction (for example, $\tau_0 \approx 1 \text{ fm}$ is usually taken for SPS Pb+Pb $158 \text{ GeV}/\text{nucl}$ collisions). Another question is - can we really use the post FO final state measurement, $\left(\frac{dE_T}{dy}\right)_{y=0}$, directly to estimate the initial energy density. Briefly speaking, this means to neglect the longitudinal expansion caused by pressure during the evolution of our fireball, which would reduce our initial energy density to the one estimated from the data by eq. (2). Therefore, one may expect that the initial energy density is larger than the one given by this simple estimate.

2.4 Bjorken model with baryon recoil

Certainly, the assumption of non-stopping partons is an idealization: from basic physical principles we may expect that if two moving quarks stretch a string between themselves with a substantial string tension, they should be decelerated, since during such a process they are converting their kinetic energy into the energy of the string. Thus, the creation of the chromoelectric field should produce some baryon recoil for both colliding nuclei. In the first approximation this was done in Ref. [34].

The authors developed the model for pA collisions. The initial momentum of the projectile, p , was considered to be so huge, that the recoil effect could be disregarded for it, while for the target partons the recoil arises from the acceleration of partons in an effective external field $F^{\mu\nu}$, produced in the collision. This baryon recoil was included in a way that guarantees the conservation of baryon current. At the same time the energy-momentum conservation was obviously violated - the effective field produced in the collision was considered to be external, and the projectile matter was not taken into account in the energy-momentum tensor of the system. Thus, the authors ended up with the following system of the modified fluid dynamical equations:

$$\partial_\mu T^{\mu\nu} = F^{\nu\mu} N_\mu + \Sigma_\pi^\nu, \quad (3)$$

$$\partial_\mu N^\mu = 0, \quad (4)$$

where $T^{\mu\nu} = e_t ((1 + c_0^2) u_t^\mu u_t^\nu - c_0^2 g^{\mu\nu})$ is an energy-momentum tensor (only target matter is taken into account), c_0^2 comes from the EoS $P = c_0^2 e$, Σ_π^ν is the pion source term [32], and $N^\mu = n u^\mu$. The effective field, $F^{\mu\nu}$, is parametrized

in the following way:

$$F^{\mu\nu} = \begin{pmatrix} 0 & 0 & 0 & -\sigma \\ 0 & 0 & 0 & 0 \\ 0 & 0 & 0 & 0 \\ \sigma & 0 & 0 & 0 \end{pmatrix}, \quad (5)$$

where $\sigma = \text{const}$ is the field strength, or string tension, of the above described effective external field. The authors have found $\sigma \approx 3 - 4 \text{ GeV}/fm$.

Without the source term the system (3, 4) can be solved analytically [34]. The source term is necessary at the later stages of the reaction, since it allows the neutralization process, i.e. the mechanism by which the energy stored in the field is converted back into the energy of matter (see [34] for details). The interplay between the baryon recoil and the energy, coming from the neutralization of the strings - string decay, leads to much higher energy density in the fragmentation region than the original Bjorken model predicts. We will come up with the modification of this nice simple model in section 3.

Experiments have now entered the region where the Bjorken model is expected to be applicable, but there is no clear and unambiguous confirmation that Nature follows this scenario. The preliminary experimental results from RHIC do not show transparency - most particle multiplicities do not show a dip in the rapidity spectra, but rather a plateau around mid-rapidity [35,36], which is a sign of strong stopping. Furthermore, a very strong elliptic flow (v_2 flow component¹) has been measured, which shows a clear peak around mid rapidity [35,40]. To build such a strong elliptic flow, strong stopping and momentum equilibration are required. Also the \bar{p}/p ratio at mid-rapidity measured at RHIC [41,42] (preliminary) is still far from one, which tells us that the middle region is not baryon-free.

¹ Nowadays the expansion in Fourier series is usually applied to study the azimuthal distribution of particles [37,38]:

$$E \frac{d^3 N}{d^3 p} = \frac{1}{\pi} \frac{d^2 N}{dp_t^2 dy} \left[1 + \sum_{n=1}^{\infty} 2v_n \cos(n\phi) \right],$$

where ϕ is the azimuthal angle. The first term in square brackets represents the isotropic radial flow, while the others are referred to anisotropic flow. The first Fourier coefficient $v_1 = \langle \cos \phi \rangle \equiv \langle p_x/p_t \rangle$ is called directed flow, and the second one $v_2 = \langle \cos(2\phi) \rangle \equiv \langle (p_x/p_t)^2 - (p_y/p_t)^2 \rangle$ is called elliptic flow.

2.5 Third flow component

As discussed in the introduction, the fluid dynamics is governed by the Equation of State of the matter, and the analysis of the resulting flow patterns turned out to be one of the best tools to extract the EoS from the outcome of a heavy ion collision. The final event shape must carry the information about the pressure development during the collision including the early stages of the collision.

The phase transition to the QGP is connected to a decrease of pressure according to most theoretical estimates, not only in strong first order phase transition models, but even if we have a smooth but rapid, gradual transition. This reduced pressure around the phase transition threshold are known for long (see e.g. [45]), and it was emphasized as a possible QGP signal: this “soft point” of the EoS might be possible to observe in excitation functions of collective flow data [48,49]. It was pointed out earlier [43] that the decrease in the out-of-plane (squeeze out) emission is even more sensitive to the pressure drop and it decreases due to plasma formation stronger than the in-plane collective flow.

In this section we want to discuss another consequence of the same softening in the EoS, which is a recently (1999) identified new distinct flow pattern - the third flow component [44]. This flow pattern can be seen in almost all theoretical fluid dynamics calculations with QGP formation, and also in experimental data, but it was not discussed earlier, see for example [43,46–48,50].

Two basic flow patterns have been predicted and detected before at lower energies:

- A) the directed transverse flow in the reaction plane, or side-splash, or bounce off, which is most frequently presented on the well known p_x vs. y diagram (or v_1 flow component vs. y) and seen at all energies in heavy ion collisions from energies of $30 A \cdot MeV$ to $165 A \cdot GeV$ [54–57];
- B) the squeeze-out effect which is an enhanced emission of particles transverse to the reaction plane at center-of-mass rapidities.

At lower energies the directed transverse flow resulted in a smooth, linear p_x vs. y dependence at CM rapidities. This straight line behavior connecting the maximum at y_{proj} and the minimum at y_{targ} was so typical that it was used to compare flow data at different beam energies and masses.

At higher energies, say above $10–11 A \cdot GeV$ in Lab frame, the deviations from this straight line behavior have been observed [51,54,56,57]. Unfortunately, directed flow has not yet been measured at RHIC.

In theoretical calculations the important feature of this third flow component is that it is clearly seen in fluid dynamical calculations when, and only when, the QGP formation was allowed during the calculation (see [44] for overview). In sharp contrast, the solutions with a purely hadronic EoS did not show this effect, and the maximum and minimum of the p_x curve could be connected with a straight line².

2.6 Possible source of the third flow component in fluid dynamics

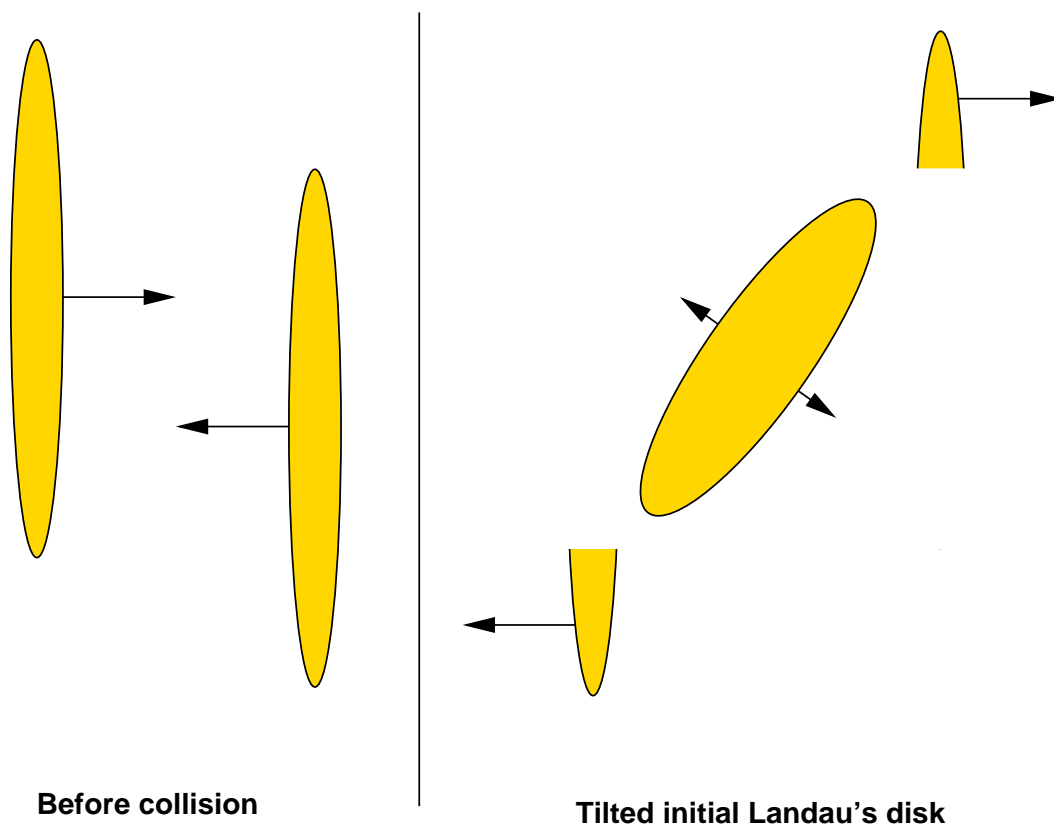


Fig. 3. Tilted initial state. The direction of the largest pressure gradient stays in the reaction plane, but deviates from both the beam and the usual transverse flow directions. Such initial conditions may lead to the creation of the third flow component [44].

The following possible source of the third flow component has been proposed in Ref. [44]. If QGP is formed in the collision, strong and rapid stopping may take place, and a behavior close to that of a one-fluid model one might be established. I.e., let's assume that Bjorken scenario is not realized, at least in

² Note that all these fluid dynamical calculations were done much before the experiments. The first quantitative flow predictions [46] preceded the experiments by six years and gave rather good agreement with the data.

its form discussed in previous section, but that the Landau fluid dynamical model is applicable for collisions of massive ultra-relativistic heavy ions (see the discussion at the end of section 2.4). The soft and compressible QGP forms a rather flat disk which is at rest in the CM system (see Fig. 3). Then this disk starts to expand in the direction of the largest pressure gradient. At small but finite impact parameters we may assume that this disk is tilted, and the direction of fastest expansion will stay in the reaction plane, but will deviate from the both beam axis and the usual transverse flow direction. Thus, a third flow component might develop from the large pressure gradient and tilted and strongly Lorentz contracted initial state. Now the flow in the reaction plane will have an “elliptic structure” [56,58,59] and must be characterized by two flow components: the usual transverse flow and the one orthogonal to it - the third flow component or antiflow. At the same time as the primary directed flow is weakened by the stronger Lorentz contraction at higher energies, this third flow component is strengthened by increased pressure gradient arising from the Lorentz contraction.

The concept of a tilted “fireball” was proposed initially in the so-called “firestreak” models [60,61]. The idea behind it is rather simple and has to do with momentum conservation. Without going into mathematical details we can understand it in the following way. First, let us create a grid in the $[x, y]$ -plane and subdivide the projectile and target into streaks parallel to the beam direction. We try to describe the collision with finite impact parameter. In the CM frame in one streak the pieces of matter from target and projectile will have the same absolute values of rapidities, but different momenta, since they in general contain different amount of matter (see Fig. 4). If the collision happens so fast that there is no interaction between streaks, then the momentum conservation does allow complete stopping, i.e., the final streak - the piece of matter within one tube with the same transverse coordinates after collision of target and projectile fragments - will have a momentum defined by momentum conservation, and correspondingly its center of mass has to move with some rapidity. Crossing the participant region along x axes in the reaction plane we will see that in the middle the final streaks rapidities are small, since the target and projectile fragments were almost equal; while at the edges of the participant region the final streaks move rather fast (see Fig. 4). Thus, after some time our tilted “fireball” will degenerate into a “firestreak”. Please notice the difference between “firestreak” and the tilted Landau disk discussed above: the tilted disk was at rest in CM frame, i.e., the complete stopping has been assumed, while “firestreak” geometry is dynamic. By “dynamic” we mean that different parts of “firestreak” move with different rapidities.

In “firestreak” models such a geometry has been assumed at the freeze-out time, and then, based on energy, charge and baryon number conservations (we already conserve momentum) the authors tried to reproduce the parameters of the post FO distribution [61]. This procedure is somewhat similar to the

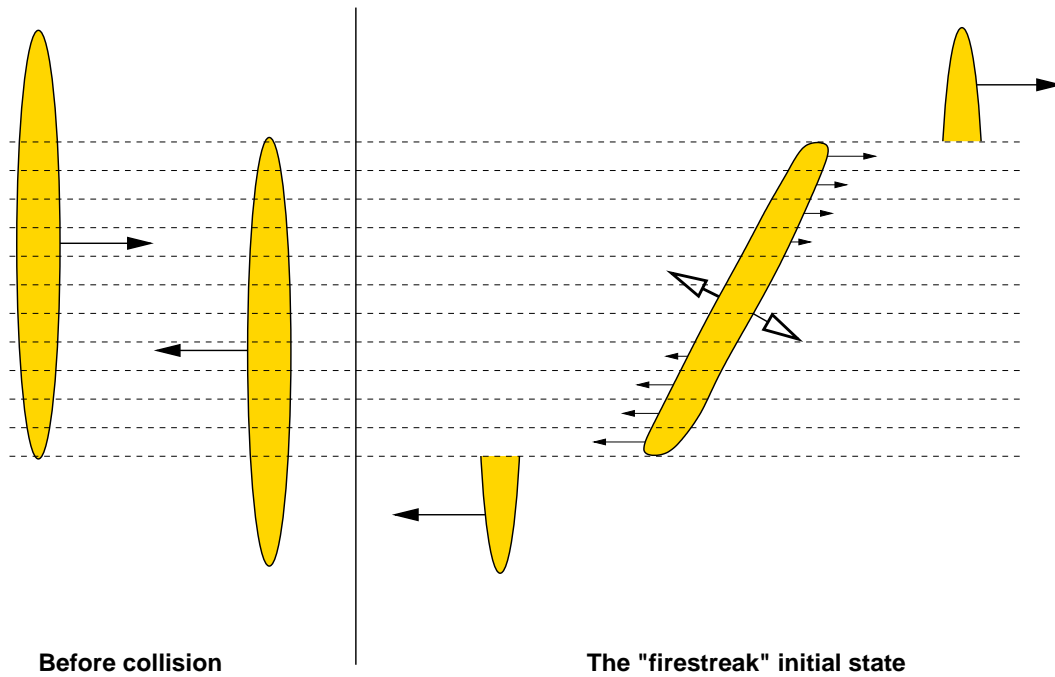


Fig. 4. The “firebreak” initial state.

statistical production model, which is used nowadays to calculate production of different hadronic species at chemical FO hypersurface. Such calculations were not really supported by experiment. Nevertheless, in our opinion, this scenario might be a good qualitative description for the initial stages of the heavy ion collisions until the local thermalization achieved. When the matter is locally thermalized and the pressure is built up, we cannot neglect hydrodynamical expansion, which will smear out this initial distribution producing a more or less spherical fireball before the freeze out process starts. Nevertheless, such a hydrodynamical expansion will initially start in the direction of the largest pressure gradient (see Fig. 4) and, together with the initial velocity field, might produce a two component (elliptic) structure of the flow in the reaction plane, identified in ref. [44].

3 Effective String Rope model

In this section we will discuss so called Effective String Rope model (ESRM) for energy, pressure and flow velocity distributions at the beginning of ultra-relativistic heavy ion collisions. The output of this model can be used as an initial condition for further hydrodynamic calculations.

One important conclusion of heavy ion research in the last decade is that standard 'hadronic' string models fail to describe heavy ion experiments. All

string models had to introduce new, energetic objects: string ropes [62,63], quark clusters [64], or fused strings [65], in order to describe the abundant formation of massive particles like strange antibaryons. Based on this, we describe the initial moments of the reaction in the framework of classical, or coherent, Yang-Mills theory, following the Bjorken model with baryon recoil Ref. [34] (see section 2.4) assuming a larger field strength (string tension) than in ordinary hadron-hadron collisions. For example, calculations both in the Quark Gluon String Model (QGSM) [66,46,67] and in the Monte Carlo string fusion model [65] indicate that the energy density of strings reaches $8 - 10 \text{ GeV}/fm$ already in SPS reactions. This is nearly 10 times more than the tension used in standard, 'hadronic', string models where $\sigma \approx 1 \text{ GeV}/fm$. In addition we now satisfy all conservation laws exactly, while in Ref. [34], as it was discussed in section 2.4, energy-momentum conservation was irrelevant and was ignored. Thus, in this approach for the first time the initial transparency/stopping and energy deposited into strings and "string ropes" was determined consistently with each other [70].

We do not describe the hadronization of our strings. Thus, this approach can be justified only for the very initial stages. The effective way to perform string decay will be discussed in section 3.3.

Recent parton kinetic models indicate that saturation of a gluon plasma takes place in a very short time - $\tau_{sat} = 0.09, 0.27 \text{ fm}/c$ for LHC, SPS energies respectively [27], and a pressure needs $\tau_p = 1 - 2 \text{ fm}/c$ (SPS) and $\tau_p = 3 - 5 \text{ fm}/c$ (LHC) to be established [39]. More importantly the first experiments at RHIC yield strong elliptic flow, which, as it was mentioned in introduction, was not reproduced in any other model, except in fluid dynamical models with a QGP EoS [35]. This is a strong experimental indication that transverse pressure builds up early in these reactions, in a few fm/c , and strong stopping is also necessary to create strong flow before Freeze Out, which usually happens when the radius of the system is not more than 10 fm . Our model builds up the locally equilibrated matter - the initial conditions for further hydrodynamical expansion - at $t_{lab} = 3/5 \text{ fm}/c$ for central/peripheral regions at RHIC energies, which is in agreement with previous estimations as well as the data.

The presentation in this section is based on Refs. [68–70], but we want to stress that the preliminary results were presented at conferences and published in their proceedings, while the model was still being developed and, thus, Ref. [70] is more up to date than Refs. [68,69]. And in this work we also improved the presentation of our model, particularly in sections 3.3, 3.4, 3.5. For the continuous description we will repeat in this section some details from Ref. [70], but we will also underline the differences.

3.1 Formulation of model

The basic idea is to generalize the Bjorken model with baryon recoil, presented in section 2.4, for collisions of two heavy ions and improve it by strictly satisfying conservation laws [68–70]. Similar ideas were also presented recently in [71].

First of all, we would like to create a grid in the $[x, y]$ -plane (z is the beam axes, $[z, x]$ is the reaction plane). We will describe the nucleus-nucleus collision as a sum of independent streak-by-streak collisions corresponding to the same transverse coordinates, $\{x_i, y_j\}$. We assume that baryon recoil for both target and projectile arise from the acceleration of partons in an effective field, $F^{\mu\nu}$, produced in the interaction. Of course, the physical picture behind this model is based on chromoelectric flux tube or string models, but for our purpose we consider $F^{\mu\nu}$ as an effective Abelian field. The most important consequence of the non-Abelian fields, i.e., its self interaction and the resulting flux tubes of constant cross section, are, nevertheless, reflected in our model: we assume that the field is one-dimensional. The fields generated by the colliding streaks are of constant cross section during the whole evolution, and only their lengths increase with time. As the string tension is constant, the energy of the string increases linearly with increasing length. The single phenomenological parameter we use to describe this field must be fixed from comparison with experimental data.

We describe the streak-streak collision based on the following set of equations:

$$\partial_\mu \sum_i T_i^{\mu\nu} = \sum_i F_i^{\nu\mu} q_i N_{i\mu} , \quad (6)$$

$$\partial_\mu \sum_i N_i^\mu = 0 , \quad i = 1, 2 , \quad (7)$$

where N_i^μ is the baryon current of i th nucleus, q_i is the color charge (discussed later in more detail). We are working in the Center of Rapidity Frame (CRF), which is the same for all streaks. We will use the parameterization:

$$N_i^\mu = n_i u_i^\mu , \quad u_i^\mu = (\cosh y_i, \sinh y_i) . \quad (8)$$

$T^{\mu\nu}$ is the energy-momentum tensor. It consists of five parts, corresponding to two nuclei and free field energy (also divided into two parts) and one term defining the QCD perturbative vacuum. (While in the similar equation in the Bjorken model with baryon recoil, eq. (3), $T^{\mu\nu}$ contains only the target matter.)

$$T^{\mu\nu} = \sum_{i=1,2} T_i^{\mu\nu} + T_{pert}^{\mu\nu} =$$

$$\sum_{i=1,2} \left[e_i \left((1 + c_0^2) u_i^\mu u_i^\nu - c_0^2 g^{\mu\nu} \right) + T_{F,i}^{\mu\nu} \right] + B g^{\mu\nu} . \quad (9)$$

Here B is the bag constant, the equation of state is $P_i = c_0^2 e_i$, where e_i and P_i are the energy density and pressure of QGP.

Comparing our equation (6) with the corresponding one in the Bjorken model with baryon recoil, eq. (3), one may notice that we neglected the pion source term. As it was discussed in section 2.4 the source term takes care about the string hadronization process. We are planning to use our model at the beginning of the ultra-relativistic heavy ion collisions only, and the string decay process at later stages will be described separately. Section 3.3 is devoted to this question. The advantage of equations (6, 7) is a simple analytic solution.

Within each streak we form only one flux tube with uniform field strength or field tension, σ , between the target and the projectile streaks. The field extends to the outside edges of the target and projectile streaks, i.e., the field also overlaps with the space-time domains of the matter streaks. For practical and symmetry purposes we, however, divide this field into two spatial domains, a target and a projectile domain, ($i = 1, 2$), separated at a fixed point, z_{sep} , so that $\sigma_1 = \sigma_2 = \sigma$. The choice of this point will be specified later. (The field is constant and the only change is that it extends with time at its two ends.)

In complete analogy to electro-magnetic field

$$F_i^{\mu\nu} = \partial^\mu A_i^\nu - \partial^\nu A_i^\mu = \begin{pmatrix} 0 & -\sigma_i \\ \sigma_i & 0 \end{pmatrix} , \quad (10)$$

$$\sigma_i = \partial^3 A_i^0 - \partial^0 A_i^3 , \quad (11)$$

$$T_{F,i\mu\nu} = -g_{\mu\nu} \mathcal{L}_{F,i} + \sum_{\beta} \frac{\partial \mathcal{L}_{F,i}}{\partial (\partial^\mu A_i^\beta)} \partial_\nu A_i^\beta , \quad (12)$$

$$\mathcal{L}_{F,i} = -\frac{1}{4} F_{i\mu\nu} F_i^{\mu\nu} . \quad (13)$$

In our case the string tensions, σ_i , will be constant in the space-time region after string creation and before string decay. The creation of fields will be discussed later in more detail.

Since during the interpenetration both nuclei are closely following the light cone, the geometry of the reaction suggests to use the light cone variables

$$(z, t) \rightarrow (x^+, x^-), \quad x^\pm = t \pm z , \quad (14)$$

and to assume that e_1, y_1, n_1 are functions of x^- only (the first nucleus goes from right to left, $y_1(0) = -y_0 < 0$) and e_2, y_2, n_2 depend on x^+ only (the second nucleus goes from left to right, $y_2(0) = y_0 > 0$).

In terms of lightcone variables (for the transformation matrixes between space-time and lightcone coordinates see Ref. [70]):

$$N_i^\pm = N_{i,\mp} = n_i(u_i^0 \pm u_i^3) = n_i e^{\pm y_i} , \quad (15)$$

$$T_i = \begin{pmatrix} T_i^{++} & T_i^{+-} \\ T_i^{-+} & T_i^{--} \end{pmatrix} = \frac{1}{2} \begin{pmatrix} h_{i+} e^{2y_i} & h_{i-} \\ h_{i-} & h_{i+} e^{-2y_i} \end{pmatrix} + T_{F,i} , \quad (16)$$

where

$$h_{i+} = (1 + c_0^2) e_i , \quad h_{i-} = (1 - c_0^2) e_i . \quad (17)$$

The other tensors in light cone variables are:

$$F_i = \begin{pmatrix} F_i^{++} & F_i^{+-} \\ F_i^{-+} & F_i^{--} \end{pmatrix} = \begin{pmatrix} 0 & \sigma_i \\ -\sigma_i & 0 \end{pmatrix} . \quad (18)$$

$$T_{pert} = \begin{pmatrix} 0 & B \\ B & 0 \end{pmatrix} . \quad (19)$$

The energy-momentum tensor for free field in the light cone variables is:

$$T_{F,i} = \frac{1}{2} \begin{pmatrix} \sigma_i^2 & 0 \\ 0 & \sigma_i^2 \end{pmatrix} . \quad (20)$$

At the time of the first contact of the two streaks, $t = 0$, there is no string tension. We assume that strings are created, i.e., the string tension achieves the value σ at time $t = t_0$, corresponding to complete penetration of streaks through each other (see Fig. 5).

3.2 Conservation laws and string creation

In lightcone variables eq. (7) may be rewritten as

$$\partial_- N_1^- + \partial_+ N_2^+ = 0 . \quad (21)$$

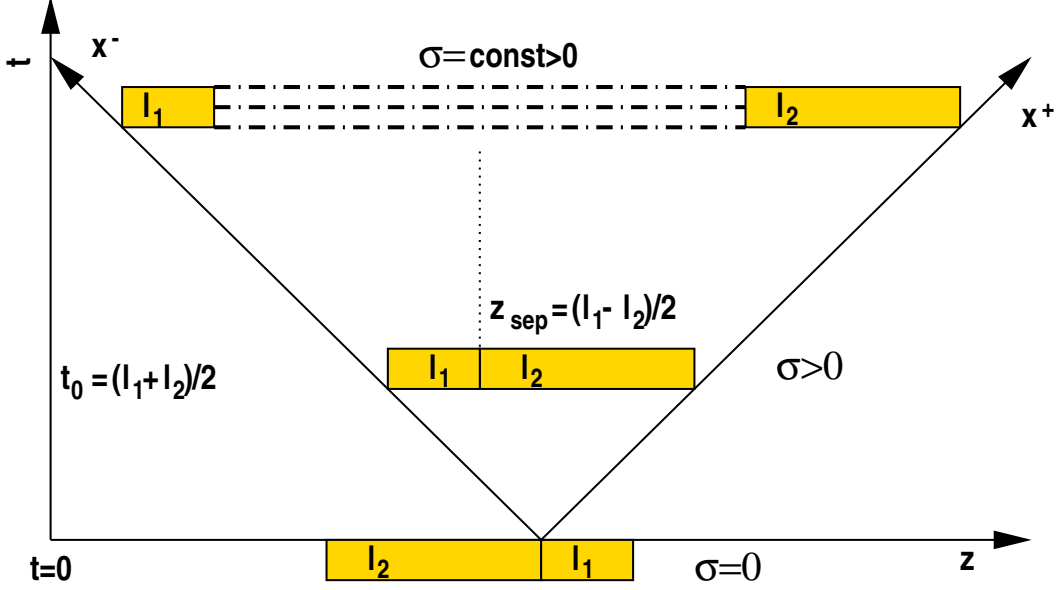


Fig. 5. Streak-streak collision. The time of first touch of streaks is $t = 0$, and $t = t_0$ corresponds to complete penetration of streaks through each other. At this time strings are created, i.e., the string tension reaches an absolute value $\sigma = A \left(\frac{\varepsilon_0}{m}\right)^2 n_0 \sqrt{l_1 l_2}$ (32). The dash-dotted lines denote the chromoelectric field strings (it will be shown later that σ is so big that we can talk about several parallel strings or a “string rope”).

So, we have a sum of two terms, each depending on different independent variables, and the solution can be found in the following way:

$$\begin{aligned} \partial_- N_1^- &= a, & \partial_+ N_2^+ &= -a, \\ N_1^- &= ax^- + (N_1^-)_0, & N_2^+ &= -ax^+ + (N_2^+)_0, \end{aligned} \quad (22)$$

where the index 0 indicates the initial proper density, which is the normal nuclear density: $n_0 = 0.145 \text{ fm}^{-3}$. Since both N_1^- and N_2^+ are positive (and also more or less symmetric) we can conclude that for our case $a = 0$.

Finally,

$$N_1^- = n_1 e^{-y_1} = n_0 e^{y_0}, \quad N_2^+ = n_2 e^{y_2} = n_0 e^{y_0}, \quad (23)$$

$$n_1 = n_0 e^{y_0 + y_1}, \quad n_2 = n_0 e^{y_0 - y_2}. \quad (24)$$

where y_0 ($-y_0$) is the initial rapidity of nucleus 2 (1) in the CRF, respectively. The other components are given by eq. (15).

Let us make an analogy to the electro-magnetic field, where two charges, q_1 and $-q_2$, move in the opposite directions, creating string-like field between them,

$\vec{E} = (0, 0, E)$, which is constrained transversally into a constant cross section. The Z -axis goes through the charges, q_1 and $-q_2$, and directed from q_1 to $-q_2$ (let us assume that we have such a field configuration). So, forces acting on our charges, $q_1 E$ and $-q_2 E$, have opposite sign and both are working against the expansion of the “string”. In our effective model we use color charges, and assume that the vectors of these color charges point in the opposite directions in the color space [65], so that the forces acting on both target and projectile partons are opposite, both stopping the expansion of the streak. As our field strength (string tension, σ) is not yet defined we normalize the charges to unity:

$$q_1 = -q_2 = 1 > 0, \quad \text{while} \quad \sigma_1 = \sigma_2 = \sigma. \quad (25)$$

Then, we have the forces acting in z direction: $q_1 \sigma_1 = \sigma$, and $q_2 \sigma_2 = -\sigma$. Notice again that after string creation fields $\sigma_1(x)$ and $\sigma_2(x)$ are spatially separated as well as the baryon densities, n_1 and n_2 ; i.e., after complete penetration of the initial streaks through each other (see Fig. 5), σ_2 acts on the partons on the right side of the separating point $z_{sep} = (l_1 - l_2)/2$, while the σ_1 acts on those on the left side. In the absence of matter, in the middle both fields are identical, so the exact position of the separating point does not play any role until it does not enter the target or projectile matter. The fields σ_i are generated by the corresponding four-potentials A_i , which are different and spatially separated in the same way (see the dotted separating line, $z_{sep} = (l_1 - l_2)/2$, in Fig. 5).

As described above we do not generate the chromoelectric field self-consistently as a product of color currents, which are also affected by the field. Our effective fields are external with respect to the colliding partons; that’s why we can use the expression (20) for the field energy. On the other hand, if we want to satisfy the conservation laws, we must generate our effective fields in the collision transferring energy from matter to field. It’s possible to define new conserved quantities based on eq. (6). Using the definition of $F^{\mu\nu}$, eq. (11), we can rewrite eq. (6) as

$$\begin{aligned} \partial_\mu T^{\mu\nu} &= \sum_i F_i^{\mu\nu} q_i N_{i,\mu} = \sum_i q_i [\partial^\mu (A_i^\nu N_{i,\mu}) - \\ &- A_i^\nu \partial^\mu N_{i,\mu} - \partial^\nu (A_i^\mu N_{i,\mu}) + A_i^\mu \partial^\nu N_{i,\mu}] . \end{aligned} \quad (26)$$

The solutions for N_1^- and N_2^+ , eq. (23), show that the second term vanishes. The fourth term is a vector $(A_1^- \partial_- N_1^+, -A_2^+ \partial_+ N_2^-)$ in lightcone coordinates. So, if we impose the conditions

$$A_1^- = 0, \quad A_2^+ = 0 \quad (27)$$

we can define a new energy-momentum tensor $\tilde{T}^{\mu\nu}$, such that

$$\partial_\mu \tilde{T}^{\mu\nu} = 0, \quad (28)$$

$$\begin{aligned} \tilde{T}^{\mu\nu} &= \sum_i \tilde{T}_i^{\mu\nu} + T_{pert}^{\mu\nu} = \\ &= \sum_i (T_i^{\mu\nu} - q_i A_i^\nu N_i^\mu + g^{\mu\nu} q_i A_i^\alpha N_{i\alpha}) + B g^{\mu\nu} \end{aligned} \quad (29)$$

One may notice that the above defined new energy-momentum tensor is not symmetric. We know that the energy-momentum tensor is not defined in unique way - if $T^{\mu\nu}$ satisfies the eq. $\partial_\mu T^{\mu\nu} = 0$, then any other tensor $T^{\mu\nu} + \partial_\kappa \Psi^{\mu\nu\kappa}$, satisfies it also, if $\Psi^{\mu\nu\kappa} = -\Psi^{\nu\mu\kappa}$ [72]. How to make it symmetric will be discussed later in this section.

To satisfy the above choice of the fields, (25), and imposed conditions, (27), we take the vector potentials in the following form:

$$\begin{aligned} A_1^- &= 0, & A_1^+ &= -\sigma_1 x^+ = -\sigma x^+, \\ A_2^- &= \sigma_2 x^- = \sigma x^-, & A_2^+ &= 0. \end{aligned} \quad (30)$$

In principle the vector potentials are not defined in unique way - the general expression would be:

$$\begin{aligned} A_1^- &= 0, & A_1^+ &= -\sigma x^+ + a_1 x^-, \\ A_2^- &= \sigma x^- + a_2 x^+, & A_2^+ &= 0. \end{aligned} \quad (31)$$

In our published work, Ref. [70], the choice $a_1 = a_2 = 0$ has been used. It appears that this intuitive choice has a deep meaning - with any other a_1 and a_2 the symmetrization procedure, which will be discussed below, can not be applied.

How to define the σ itself? In our calculations we used the parameterization (see Refs. [68–70]):

$$\sigma = A \left(\frac{\varepsilon_0}{m} \right)^2 n_0 \sqrt{l_1 l_2} = A \left(\frac{\varepsilon_0}{m} \right) \frac{\sqrt{n_1 n_2}}{\Delta x \Delta y}, \quad (32)$$

where m is the nucleon mass, ε_0 is the initial energy per nucleon, l_1 and l_2 are the initial streak lengths in the CRF (see Fig. 5), n_1 and n_2 are the numbers of baryons in the initial streaks, $\Delta x \Delta y$ is the cross section of the

streaks, and we've used the relation $\gamma = \varepsilon_0/m$. Similar $(\mathbf{n}_1, \mathbf{n}_2)$ -dependence of $\sigma =$ has been chosen in Ref. [71]. We are working in the system where $\hbar = c = 1$, so σ has a dimension of $length^{-2} = energy/length$. The typical values of dimensionless parameter A are around $0.06 - 0.08$ (these values of A are for σ measured already in GeV/fm). Notice, that there is only one free parameter in parameterization (32). The typical values of σ are $4-10 GeV/fm$ for $\varepsilon_0 = 65 GeV$ per nucleon, and $\sigma \approx 6 - 15 GeV/fm$ for $\varepsilon_0 = 100 GeV$ per nucleon. These values are consistent with the energy density of the non-hadronized strings in a reaction volume, or "latent energy density", which is about $15 GeV/fm^3$ for $\sqrt{s} = 200 GeV/nucleon$ [46,66,67]. Our σ given by eq. (32) grows linearly with ε_0 . This may be a too strong assumption, since we predict much bigger field strength for LHC then the Monte Carlo string fusion model [65]. It is easy to modify expression (32) by changing the power 2 to $1 + \alpha$, where $\alpha < 1$, and probably this will be done after the comparison with experimental data. In Ref. [71] $\alpha = 0.3$ has been chosen based on the low- x behavior of the nuclear structure function or parton density [73]. Since such an improvement is straightforward, we will keep it in mind, but for further discussion we will use the definition (32) as in Ref. [68–70].

Using the exact definition of A_i^μ , eqs. (30), eqs. (16, 19, 20, 25, 29) and transformation matrixes from Ref. [70] we obtain

$$\begin{aligned} \tilde{T}^{\mu\nu} &= \begin{pmatrix} \tilde{T}^{++} & \tilde{T}^{+-} \\ \tilde{T}^{-+} & \tilde{T}^{--} \end{pmatrix} = \frac{1}{2} \begin{pmatrix} h_{1+}e^{2y_1} & h_{1-} \\ h_{1-} & h_{1+}e^{-2y_1} \end{pmatrix} \\ &+ \frac{1}{2} \begin{pmatrix} h_{2+}e^{2y_2} & h_{2-} \\ h_{2-} & h_{2+}e^{-2y_2} \end{pmatrix} + \frac{1}{2} \begin{pmatrix} \sigma^2 & 2B \\ 2B & \sigma^2 \end{pmatrix} \\ &+ \begin{pmatrix} -\sigma x^+ N_1^+ & 0 \\ \sigma x^+ N_1^- & 0 \end{pmatrix} + \begin{pmatrix} 0 & \sigma x^- N_2^+ \\ 0 & -\sigma x^- N_2^- \end{pmatrix} \end{aligned} \quad (33)$$

Notice that the perturbative vacuum term, B , and the free field energy, $\frac{\sigma^2}{2}$, cover all the interacting volume, while the energy densities of matter and baryon currents are separated in space.

Now we are coming back to the question: how to symmetrize $\tilde{T}^{\mu\nu}$? One may notice that the tensor

$$\tilde{T}_1^{\mu\nu} = \begin{pmatrix} 0 & \sigma x^- N_2^+ \\ \sigma x^+ N_1^- & 0 \end{pmatrix}, \quad (34)$$

satisfies the equation $\partial_\mu \tilde{T}_1^{\mu\nu} = 0$ (it's easy to check using the eqs. (23)). Thus we can redefine $\tilde{T}^{\mu\nu}$ in a symmetric way:

$$\tilde{T}^{\mu\nu} := \tilde{T}^{\mu\nu} - \tilde{T}_1^{\mu\nu} . \quad (35)$$

This important step has not been done in Refs. [68–70]. It causes some changes in the calculations of the energy densities at $t = t_0$ (see A), but we will see that this does not affect appreciably the final results.

Now the new conserved quantities are

$$Q^0 = \int \tilde{T}^{00} dV = \Delta x \Delta y \int \tilde{T}^{00} dz , \quad (36)$$

$$Q^3 = \int \tilde{T}^{03} dV = \Delta x \Delta y \int \tilde{T}^{03} dz . \quad (37)$$

We can rewrite the energy-momentum tensor in (t, z) coordinates:

$$\begin{aligned} \tilde{T}^{\mu\nu} &= \begin{pmatrix} \tilde{T}^{00} & \tilde{T}^{03} \\ \tilde{T}^{30} & \tilde{T}^{33} \end{pmatrix} = \begin{pmatrix} \frac{\sigma^2}{2} + B & 0 \\ 0 & \frac{\sigma^2}{2} - B \end{pmatrix} + \\ &\begin{pmatrix} (e_1 + P_1) \cosh^2 y_1 - P_1 & (e_1 + P_1) \cosh y_1 \sinh y_1 \\ (e_1 + P_1) \cosh y_1 \sinh y_1 & (e_1 + P_1) \sinh^2 y_1 + P_1 \end{pmatrix} + \\ &\begin{pmatrix} (e_2 + P_2) \cosh^2 y_2 - P_2 & (e_2 + P_2) \cosh y_2 \sinh y_2 \\ (e_2 + P_2) \cosh y_2 \sinh y_2 & (e_2 + P_2) \sinh^2 y_2 + P_2 \end{pmatrix} \\ & - \frac{\sigma x^+}{2} \begin{pmatrix} N_1^+ & N_1^+ \\ N_1^+ & N_1^+ \end{pmatrix} - \frac{\sigma x^-}{2} \begin{pmatrix} N_2^- & -N_2^- \\ -N_2^- & N_2^- \end{pmatrix} . \end{aligned} \quad (38)$$

Obviously, in the absence of the fields, before string creation and after string decay, $\tilde{T}^{\mu\nu} \equiv T^{\mu\nu}$ and, thus, (Q^0, Q^3) reverts to (P^0, P^3) - components of the four-momenta of the system.

Based on conservation of Q^0 , Q^3 we can calculate energy densities, $e_1(t_0)$, $e_2(t_0)$, at the moment $t = t_0$, when the string with tension σ is created - eqs. (A.13, A.14). Another result from A we will need for later discussion is the rapidity of the CM frame:

$$\tanh y_{CM} = Q^3/Q^0 = v_0/M , \quad (39)$$

where $M = \frac{l_2+l_1}{l_2-l_1}$.

Thus, for $x^\pm > x_0$ we should solve eqs. (28), with boundary conditions

$$\begin{aligned}
N_1^\pm(x^- = x_0) &= n_0 e^{\mp y_0} & N_2^\pm(x^+ = x_0) &= n_0 e^{\pm y_0} \\
h_{1+}(x^- = x_0) &= e_1(t_0)(1 + c_0^2) & h_{2+}(x^+ = x_0) &= e_2(t_0)(1 + c_0^2) \\
y_1(x^- = x_0) &= -y_0 & y_2(x^+ = x_0) &= y_0 \\
\sigma_1(x^- = x_0) &= \sigma & \sigma_2(x^+ = x_0) &= \sigma \\
q_1(x^- = x_0) &= 1 & q_2(x^+ = x_0) &= -1,
\end{aligned} \tag{40}$$

where $x_0 = 2t_0 - |z(0)|$ defines the string creation surface $t = t_0$, for a parton or cell element in the position $z = z(0)$ at the time $t = 0$. The complete analytical solution can be found in Ref. [70].

3.3 Hadronization of the String Ropes

If we let the partons (or cell domains) evolve according to trajectories derived in our model (see eqs. (37, 38) in Ref. [70]), the partons from the colliding initial streaks will keep going in the initial direction, gradually slowing down up to some time $t = t_{i,turn}$; then they will turn and go backwards until the two streaks again penetrate through each other (see Fig. 6). Of course, it is hard to believe that such a contraction of the reaction volume could really happen in heavy ion collisions, because of string decays, string-string interaction, interaction between streaks and other reasons, which would be very difficult to take into account. As we already pointed out earlier we did not install any string hadronization mechanism in our model and, thus, there is no way to decrease the energy supplied in the strings. If we try to describe the evolution of the system with our model after one or both initial streaks turn back, we run into the trouble, since the length of the string starts to decrease, so the field energy should also decrease, but it has no chance to do this. Therefore the above simple analytical model fails to describe the Yo-Yo motion for the initial streaks - it has the realistic character until the length of the final streak has started to decrease, i.e., approximately up to the dash-dotted line in Fig. 6.

In Refs. [68–70] we assumed that the final result of the collision of two streaks, after stopping the string's expansion and after its decay, is one streak of the length Δl_f with homogeneous energy density distribution, e_f , moving like one object with rapidity y_f . We assumed that this is due to string-string interactions and string decays, which we are not going to describe in our simple model. As mentioned above the typical values of the string tension, σ , are of

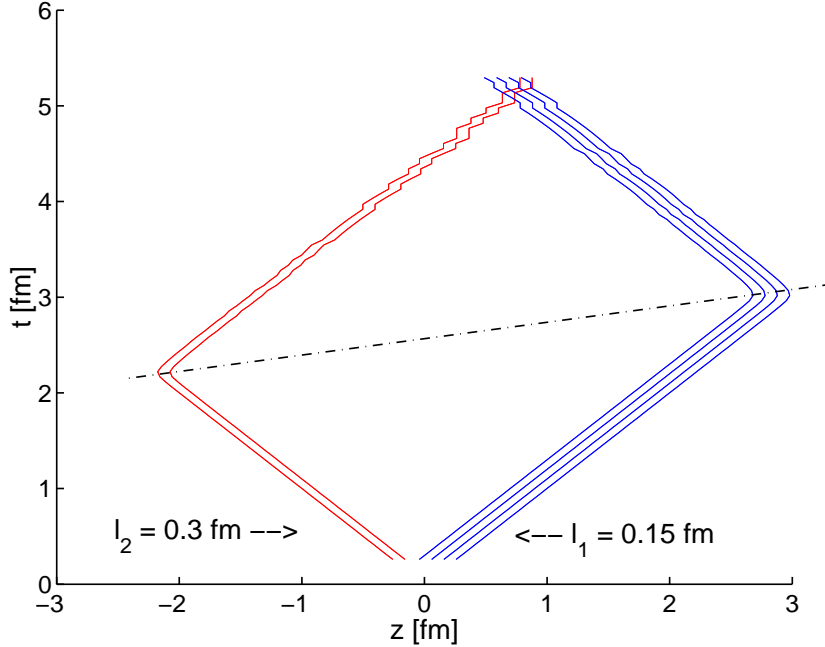


Fig. 6. The typical trajectory of the initial streaks with lengths l_1 (coming from the right) and l_2 (coming from the left).

the order of $10 \text{ GeV}/\text{fm}$, and these may be treated as several parallel strings. The string-string interaction will produce a kind of “string rope” between our two streaks, which is responsible for final energy density distribution.

One of the simplest ways to quantitatively take into account string decays is presented in Ref. [71]. One of the complications appearing in this case is that the hadronization of the strings has to be described in the proper time (i.e. all quantities became functions of (τ, η) , $\tau = \sqrt{t^2 - z^2}$) which is, in general, different for all the pairs of colliding streaks. Then in order to be able to transform all of the final streaks to one frame, say CRF, we would have to know the details of their dynamics for a long period of the proper time, $t = \sqrt{\tau^2 + z^2}$. Unfortunately this is not the case in real modeling, for example in Ref. [71] authors do not describe the dynamics after all the chromoelectric strings for the particular streak pair decay.

The real situation may be more complicated: when the energy accumulated in the strong color fields will be finally released in a production of $q\bar{q}$ pairs and gluons, this process may noticeably change the composition of matter as compared to the chemical equilibrium case [74]. Therefore, the matter created after the mutual stopping of interpenetrating streaks can not, in general, be described by the equilibrium EoS.

For the stopped and equilibrated matter a set of homogeneous final streaks is the simplest assumption. Its advantages are: simple expressions for e_f , y_f and a very simple way to generate an initial state for further hydrodynamical

description. We have to give only four numbers (coordinates of the ends of the final streak, z_{left} and z_{right} , e_f and y_f) for each point of a transverse grid, $\{x_i, y_j\}$. Later in section 3.5 we present an analytical solution for the expanding final streaks which seems to be more realistic. Remember - we describe the initial state which is not directly observable in experiments. Thus, even a flat initial rapidity distribution may end up after the hydrodynamical evolution in both a forward-backward peaked or a centrally peaked distribution depending on several circumstances.

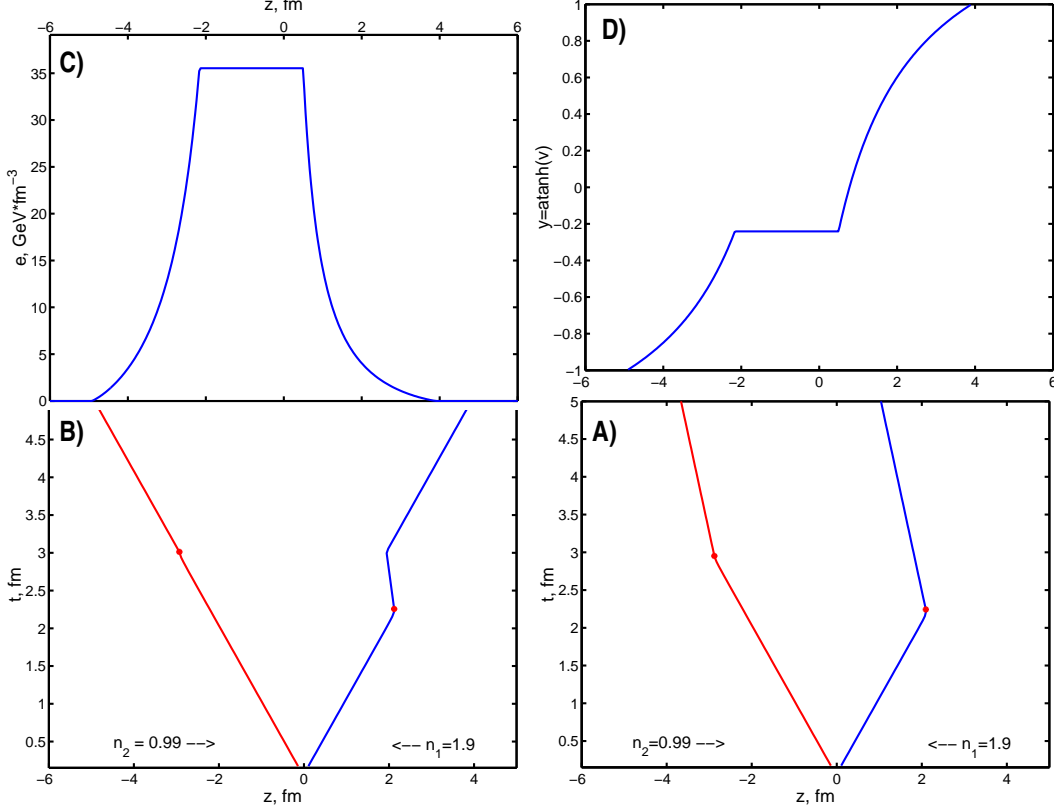


Fig. 7. A) The typical trajectory of the ends of two initial streaks corresponding to the numbers of nucleons n_1 and n_2 , $\varepsilon_0 = 65 \text{ GeV}/\text{nucl}$, $A = 0.09$ (the parameter A was introduced in eq. (32)). Stars denote the points where $y_i = y_f$. From $t = t_0$ until these stars, the streak ends move according trajectories derived in Ref. [70] (see eqs. (37, 38)). Then the final streak starts to move like a single object with rapidity y_f , eq. (41), in CRF.

B) The same situation as in subplot (A), but for expanding final streak. C) Shows $e(z)$ profiles of expanding final streak ($t_h = 5 \text{ fm}$). We can clearly see three regions - two of forward and backward rarefaction waves and a middle where the initial energy density, e_f (eq. (42)), is still preserved. D) Shows the rapidity profile of the expanding final streak ($t_h = 5 \text{ fm}$). We can clearly see three regions - two of forward and backward rarefaction waves and a middle where the initial rapidity, y_f (eq. (41)), is still preserved.

The final energy density and rapidity, e_f and y_f , should be determined from conservation laws. The conservation of the energy and momentum gives for

the final rapidity:

$$\cosh^2 y_f = \frac{(M^2(1 + c_0^2) - 2c_0^2 v_0^2) + \sqrt{(M^2(1 + c_0^2) - 2c_0^2 v_0^2)^2 + 4c_0^4 v_0^2 (M^2 - v_0^2)}}{2(1 + c_0^2)(M^2 - v_0^2)}, \quad (41)$$

where we neglected $B \Delta l_f$ next to $Q^0 / \Delta x \Delta y$ and use notation M , introduced in eq. (A.8); $v_0 = \tanh y_0$ is the initial velocity³. Then the expressions for e_f is:

$$e_f = \frac{\frac{Q^0}{\Delta x \Delta y}}{((1 + c_0^2) \cosh^2 y_f - c_0^2) \Delta l_f}. \quad (42)$$

The typical trajectory of the streak ends is presented in Fig. 7 (A). From $t = t_0$ they move according to trajectories derived in Ref. [70] (see eqs. (37, 38)) until they reach the rapidity $y_i = y_f$. Later, the final streak starts to move like one object with uniform rapidity, y_f , until we reach the time when the fluid dynamical calculation starts. The time and position of final streak formation can be found from the condition $y_i = y_f$ (see eq. (43) in Ref. [70]). We shall call this scenario the “nonexpanding final streak assumption”.

Unfortunately this simple model of the final state causes a principle problem. Comparing expressions (41) and (39) one may notice a strange thing: the final streak moves like one object with a certain rapidity calculated from energy-momentum conservation, but this rapidity, y_f , may differ, in general, from the rapidity of the Center of Mass of the system given by eq. (39). Obviously, if all the elements of the system move with the same rapidity, then the Center of Mass of the system also moves with the same rapidity. This problem have been pointed out in the Refs. [68–70], but the above oversimplified assumptions have been kept because of the simple analytical solution for the e_f, y_f . We think that now we have a deeper understanding of the source of the problem and we would like to update the discussion in Ref. [68–70]. This is illustrated and elucidated in next section.

3.4 Flow velocity field generated by pressure in relativistic fluid mechanics

Let us propose to the reader the following problem:

³ Please notice the misprint in equation for $\cosh^2 y_f$ in Refs. [68–70]: $(M^2(1 + c_0^2) + 2c_0^2 v_0^2)$ instead of $(M^2(1 + c_0^2) - 2c_0^2 v_0^2)$.

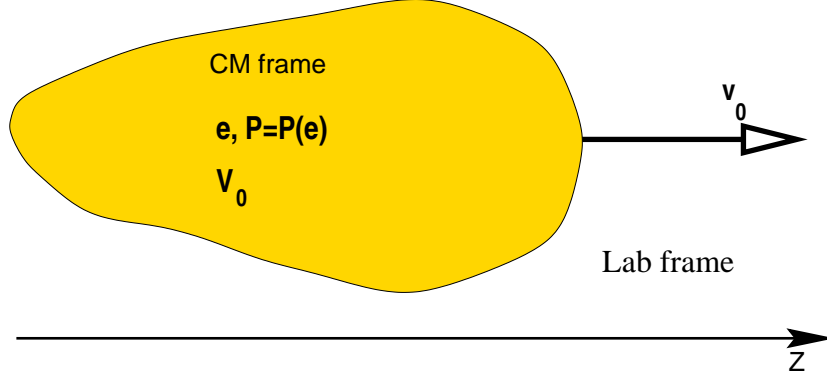


Fig. 8. The homogeneous piece of matter with energy density e and EoS $P = P(e)$ moving with velocity v_0 in the Lab frame.

Imagine the homogeneous piece of matter with energy density e and Equation of State $P = P(e)$ moving with velocity v_0 in the Lab frame (see Fig. 8). The question is to find the energy-momentum tensor, $T^{\mu\nu}$, and four-momentum, P^μ , in the Center of Mass frame and in the Lab frame and show that they are consistent with each other.

3.4.0.1 CM frame: In the CM frame, which is in our case the rest frame of matter the energy momentum tensor and four-momentum of the system are:

$$T^{\mu\nu} = \begin{pmatrix} e & 0 & 0 & 0 \\ 0 & P & 0 & 0 \\ 0 & 0 & P & 0 \\ 0 & 0 & 0 & P \end{pmatrix}, \quad (43)$$

$$P^\mu = (E, 0, 0, 0), \quad (44)$$

where $E = eV_0$, V_0 is the volume of our matter in the CM frame, $\mu, \nu = 0, 1, 2, 3$.

The four-momentum is connected to the energy-momentum tensor in the following way [72]:

$$P^\mu = \int T^{\mu\nu} dS_\nu, \quad (45)$$

where the integral is over any 3-dimensional hypersurface covering all the volume, i.e., intersecting all the world lines of the matter in space-time. If we

integrate over the hyperplane $x^0 = t = \text{const}$, then

$$P^\mu = \int T^{\mu 0} dV . \quad (46)$$

It's easy to check that equations (43) and (44) are indeed connected by the relation (46) for any EoS.

3.4.0.2 Lab frame: In the Lab frame our system is moving with velocity $\vec{v} = (0, 0, v_0)$. The four-momentum undergoes the Lorentz transformation:

$$P_L^\mu = (E\gamma_0, 0, 0, E\gamma_0 v_0) . \quad (47)$$

The invariant expression for the energy-momentum tensor in any reference frame is

$$T^{\mu\nu} = (e + P)u^\mu u^\nu - P g^{\mu\nu} . \quad (48)$$

In our case $u^\mu = \gamma_0(1, 0, 0, v_0)$. Thus,

$$T_L^{\mu\nu} = \begin{pmatrix} (e + P)\gamma_0^2 - P & 0 & 0 & (e + P)\gamma_0^2 v_0 \\ 0 & P & 0 & 0 \\ 0 & 0 & P & 0 \\ (e + P)\gamma_0^2 v_0 & 0 & 0 & (e + P)\gamma_0^2 v_0^2 + P \end{pmatrix} , \quad (49)$$

Now we have to use eq. (46) to find P_L^μ from $T_L^{\mu\nu}$.

$$P_L^0 = \int dV [(e + P)\gamma_0^2 - P] = [(e + P)\gamma_0^2 - P] V_0/\gamma_0 , \quad (50)$$

$$P_L^3 = \int dV (e + P)\gamma_0^2 v_0 = (e + P)\gamma_0^2 v_0 V_0/\gamma_0 , \quad (51)$$

where V_0/γ_0 is the volume of our system in Lab frame. Comparing eqs. (50, 51) with eq. (47) we obtain the following system of equations:

$$\begin{cases} \frac{(e+P)\gamma_0^2 - P}{\gamma_0} = e\gamma_0 \\ (e + P)\gamma_0 v_0 = e\gamma_0 v_0 \end{cases} \quad (52)$$

and we see that for a consistent description we have to put $P = 0$. Why do we get such a strong restriction on our EoS?!

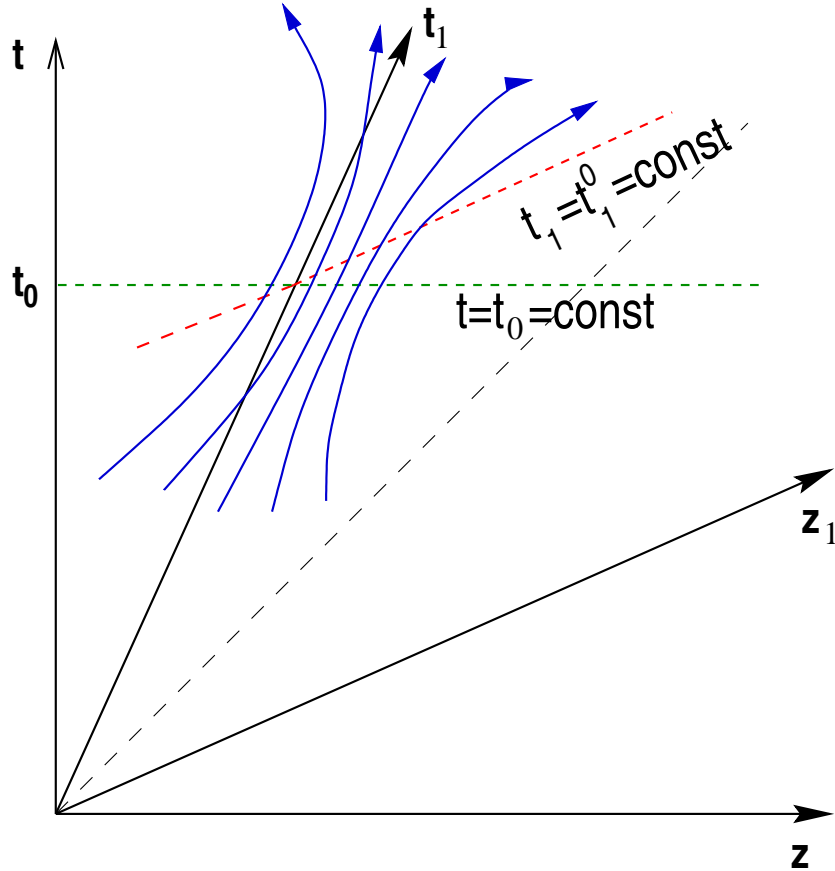


Fig. 9. All the matter on the hypersurface $t = t_0$ in the Lab frame has the same velocity, but in the CM frame on the hypersurface $t_1 = t_1^0$ different parts of matter have different velocities.

Certainly the problem is that we made wrong assumptions. We assumed that all the parts of our system are moving with the same velocity. This is true for the dust, where the pressure is exactly zero. If $P > 0$ such a situation may happen for some particular t in the particular reference frame (remember we integrate $T^{\mu\nu}$ over the hypersurface $t = const$). If we boost our system the parts of matter on the new integration hypersurface $t_1 = const$ will not move with the same velocity, as illustrated in Fig. 9: in the Lab frame all the matter on the hypersurface $t = t_0$ has the same velocity, but in the CM frame we have to either integrate over hypersurface $t_1 = t_1^0$, where different parts of matter have different velocities or integrate over hypersurface $t = t_0$ homogeneous in velocity, but in this case $dS_\mu \neq (dV, \vec{0})$ in eq. (45). Briefly speaking the presence of pressure requires, in general, the flow velocity field in CM frame, $\vec{v}_{CM}(t, \vec{r})$, for real physical situation, and our invariant energy-momentum tensor, $T^{\mu\nu}$, defined by eq. (48) seems to be clever enough to know that.

Thus, as we see, the assumption of the final streak moving like one object oversimplifies the real physical situation. The way to improve the model is to

let the final streak expand with the rapidity field which will allow us to satisfy exactly all the conservation laws. We can describe such a streak expansion based on the analytical solution for one-dimensional expansion of matter into the vacuum.

3.5 Expanding final streaks

Apart of the principal reasons discussed above, our test results [79,80] indicated that the uniform final streaks without expansion lead to somewhat unrealistic expansion patterns. Thus we had to improve the model and include the expansion of the final streaks.

In this section we discuss the one-dimensional expansion of the finite streak into the vacuum (generalizing the description in [81]). The initial condition is

$$e(z, t_0) = \begin{cases} 0 & -\infty < z < R_- , \\ e_0 , & R_- \leq z \leq R_+ \\ 0 & , R_+ < z < \infty , \end{cases} \quad (53)$$

$$v(z, t_0) = \begin{cases} -1 & , -\infty < z < R_- \\ \tanh y_0 , & R_- \leq z \leq R_+ \\ 1 & , R_+ < z < \infty , \end{cases} \quad (54)$$

where R_- , R_+ are the borders of the system. The choice $v = \pm 1$ in the vacuum is purely conventional, but it guarantees a continuous hydrodynamic solution at the boundary to the vacuum, since in the limit of infinite dilution the velocity of matter approaches unity.

Now consider a simple wave, i.e., continuous hydrodynamic flow. This flow respects entropy conservation [82]. For isentropic flow, the t - and z -component of the equation of motion, $\partial_\mu T^{\mu\nu} = 0$, can be combined to yield

$$\left(\frac{\partial}{\partial t} + \frac{v \pm c_0}{1 \pm v c_0} \frac{\partial}{\partial z} \right) \mathcal{R}_\pm = 0 , \quad (55)$$

where the so-called *Riemann invariants* are

$$\mathcal{R}_\pm \equiv y - y_0 \pm \int_{e_0}^e \frac{c_0 de'}{e' + p(e')} . \quad (56)$$

Obviously, the Riemann invariants are constant,

$$\left. \frac{d\mathcal{R}_\pm}{dt} \right|_{\mathcal{C}_\pm} = 0, \quad (57)$$

along the so-called characteristic curves $\mathcal{C}_\pm(x, t)$, the positions $x_\pm(t)$ of which are determined by integrating

$$\frac{dx_\pm}{dt} = \frac{v \pm c_0}{1 \pm vc_0}. \quad (58)$$

The characteristics are the world-lines of sonic disturbances on the hydrodynamic flow pattern. For simple waves moving to the right (i.e., $v > 0$), one can prove [83] that $\mathcal{R}_+ = \text{const}$, and it suffices to consider the \mathcal{C}_- -characteristic. For simple waves moving to the left ($v < 0$), $\mathcal{R}_- = \text{const}$, and only the \mathcal{C}_+ -characteristics have to be considered.

For the initial conditions (53, 54) we determine the value of \mathcal{R}_\pm at $t = t_0$, $z = R_\pm$ to be $\mathcal{R}_\pm = 0$ and thus

$$y_\pm = y_0 \mp \int_{e_0}^e \frac{c_0 de'}{e' + p(e')}. \quad (59)$$

If we consider the QGP EoS, $p(e) = c_0^2 e$, $c_0^2 = \text{const}$, this gives

$$\begin{aligned} v(e)_\pm &= \tanh y(e)_p m = \tanh \left[y_0 \mp \frac{c_0}{1 + c_0^2} \ln \left\{ \frac{e}{e_0} \right\} \right] = \\ &= \frac{\tanh y_0 \mp \frac{1 - (e/e_0)^{2c_0/(1+c_0^2)}}{1 + (e/e_0)^{2c_0/(1+c_0^2)}}}{1 \mp \tanh y_0 \frac{1 - (e/e_0)^{2c_0/(1+c_0^2)}}{1 + (e/e_0)^{2c_0/(1+c_0^2)}}}. \end{aligned} \quad (60)$$

This equation nicely shows the defining property of a simple wave, namely that there is a unique relationship between the value of the fluid velocity and its thermodynamic state [83]. Furthermore, with the help of (58) for \mathcal{C}_\mp , we can now calculate for any given e , $0 \leq e \leq e_0$, the position $z(t; e)$ at which this value for the energy density occurs for given t ,

$$z_\pm(t; e) - R_\mp = \frac{v(e) \pm c_0}{1 \pm v(e) c_0} (t - t_0). \quad (61)$$

Eq. (61) has similarity form, i.e., the profile of the rarefaction wave does

not change with time when plotted as a function of the similarity variable $\zeta_{\pm} \equiv \frac{z \mp R_{\pm}}{t - t_0}$.

Let us now complete the solution of the hydrodynamic problem. Causality requires that the initial conditions (53, 54) remain unchanged for $|\zeta_{\pm}| > 1$. Thus, we only have to determine the solution in the range $-1 \leq \zeta_{\pm} \leq 1$, i.e. in the forward light cone (remember that ζ_+ (ζ_-), obtained from the \mathcal{C}_- (\mathcal{C}_+)-characteristic, eq. (61), corresponds to y_+ (y_-), obtained from $\mathcal{R}_+ = \text{const}$ ($\mathcal{R}_- = \text{const}$) condition).

For the forward going rarefaction wave, $v > 0$, generated on the right end of the initial streak, from eqs. (60, 61) we infer that the head of this wave (the point where the rarefaction of matter starts, i.e., where the energy density e starts to fall below e_0) travels with the velocity $\frac{\tanh y_0 - c_0}{1 - c_0 \tanh y_0}$ to the left. On the other hand, the base of the rarefaction wave (the point where the vacuum ends, i.e., where e starts to acquire non-vanishing values) travels with light velocity $v = 1$ to the right. Thus, the energy density as a function of ζ can be written as

$$e(\zeta_+) = e_0 \cdot \begin{cases} 1, & \\ -1 \leq \zeta_+ \leq \frac{\tanh y_0 - c_0}{1 - c_0 \tanh y_0} \\ \left[\frac{1 + \tanh y_0}{1 - \tanh y_0} \frac{1 - c_0}{1 + c_0} \frac{1 - \zeta_+}{1 + \zeta_+} \right]^{(1+c_0^2)/2c_0}, & \\ \frac{\tanh y_0 - c_0}{1 - c_0 \tanh y_0} < \zeta_+ \leq 1. & \end{cases}, \quad (62)$$

The velocity can then be inferred from (60), or simply from (61):

$$\tanh y(\zeta_+) = \begin{cases} \tanh y_0, & -1 \leq \zeta_+ \leq \frac{\tanh y_0 - c_0}{1 - c_0 \tanh y_0} \\ \frac{c_0 + \zeta_+}{1 + \zeta_+ c_0}, & \frac{\tanh y_0 - c_0}{1 - c_0 \tanh y_0} < \zeta_+ \leq 1. \end{cases} \quad (63)$$

The similar analyzes for the backward going rarefaction wave, $v < 0$, generated on the left end of the initial streak, gives:

$$e(\zeta_-) = e_0 \cdot \begin{cases} 1, & \\ \frac{\tanh y_0 + c_0}{1 + c_0 \tanh y_0} \leq \zeta_- \leq 1 \\ \left[\frac{1 - \tanh y_0}{1 + \tanh y_0} \frac{1 - c_0}{1 + c_0} \frac{1 + \zeta_-}{1 - \zeta_-} \right]^{(1+c_0^2)/2c_0}, & \\ -1 < \zeta_- \leq \frac{\tanh y_0 + c_0}{1 + c_0 \tanh y_0}, & \end{cases}, \quad (64)$$

$$\tanh y(\zeta_-) = \begin{cases} \tanh y_0 & , \quad \frac{\tanh y_0 + c_0}{1 + c_0 \tanh y_0} \leq \zeta_- \leq 1 \\ \frac{\zeta_- - c_0}{1 - \zeta_- c_0} & , \quad -1 < \zeta_- \leq \frac{\tanh y_0 + c_0}{1 + c_0 \tanh y_0} . \end{cases} \quad (65)$$

This simple analytical solution is valid as long as the two rarefaction waves did not overlap in the middle of the system. Further evolution becomes more complicated and doesn't have a similarity form any more.

The point where two rarefaction waves start to overlap, z_{over} , t_{over} can be found from the system

$$\begin{cases} \zeta_+(z, t) = \frac{z - R_+}{t - t_0} = \frac{\tanh y_0 - c_0}{1 - c_0 \tanh y_0} \\ \zeta_-(z, t) = \frac{z - R_-}{t - t_0} = \frac{\tanh y_0 + c_0}{1 + c_0 \tanh y_0} , \end{cases} \quad (66)$$

which gives

$$z_{over} = \frac{-R_-(1 + \tanh y_0 c_0)(\tanh y_0 - c_0)}{2c_0(1 - \tanh^2 y_0)} , \quad (67)$$

$$t_{over} = t_0 + \frac{(z_{over} - R_+)(1 - \tanh y_0 c_0)}{(\tanh y_0 - c_0)} . \quad (68)$$

Thus the analytical solution (62-65) valid for $t_0 \leq t \leq t_{over}$.

For the symmetric initial state, $R_+ = -R_- = R$, eqs. (67,68) became

$$z_{over} = R \frac{\tanh y_0(1 - c_0^2)}{c_0(1 - \tanh^2 y_0)} , \quad (69)$$

$$t_{over} = t_0 + R \frac{1 - \tanh y_0 c_0}{c_0(1 - \tanh^2 y_0)} . \quad (70)$$

Thus, based on the solution presented above we can have a more advanced description of the final streaks than the one presented in section 3.3. Let us assume that the homogenous final streaks, with some e_f , y_f , are formed in the CRF when the larger of initial streaks reach the rapidity y_f . Up to this point the fluid cell trajectories are the same as those discussed in section 3.3, but after the homogeneous final streak is formed, it starts to expand according to the simple rarefaction wave solutions presented above. Figure 7 (B) shows new

trajectories of the streak ends, and Figures 7 (C,D) present energy density and rapidity profile for this expanding streak.

Such an initial state with expanding streaks will also help to avoid the problem which may cause the development of numerical artifacts, namely a step-like in beam direction initial energy density distribution (output of ESRM): it has a jump from $e(x_i, y_j) = \text{const}$ inside the matter to 0 in the outside vacuum (of course, where is also a jump of e as a function of x, y , but it is much smoother and this is not the direction of the initial expansion). In order to avoid (or at least to suppress) the effect of this, it was proposed in Ref. [84] to smooth over initial energy density distribution, for example by a Gaussian shape. Our simple analytic solution smooths over this jump in a natural way.

3.6 Initial conditions for hydrodynamical calculations

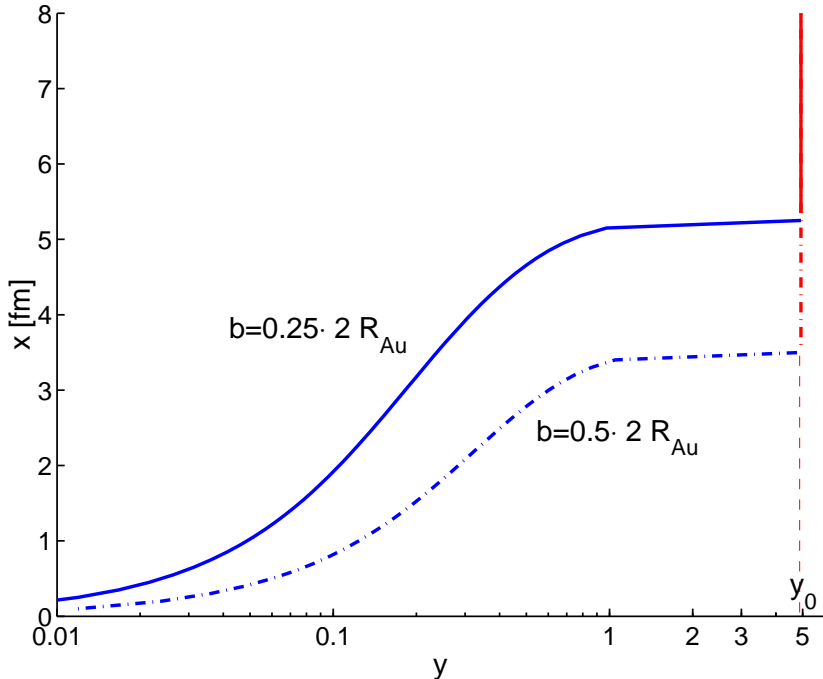


Fig. 10. Final rapidity, y_f , profiles of the final streaks in the reaction plane for Au+Au collision at $\varepsilon_0 = 65 \text{ GeV}/\text{nucl}$, $A = 0.08$. The rapidities of the final streaks in CRF are calculated according to eq. (41). Our profiles are in agreement with the schematic sketch in paper [76] and with the scenario discussed in “firestreak” model (see Fig. 4).

In this section we present the results of our calculations. We are interested in the shape of the QGP formed when the expansion of the combined target-projectile streaks stop and their matter is locally equilibrated. This will be the initial state for further hydrodynamical calculations. The time, t_h , at which we start the hydrodynamical description is a second (in addition to A) free

parameter of our model. Of course, t_h should be larger than the time of final streak formation, at least in the central, most hot and dense region. For the peripheral streaks the string tension is low, and the transparency is large, but peripheral matter does not play a leading role in further hydrodynamic expansion. Therefore, we will also build the final streaks (y_f, e_f) for peripheral streak-streak collisions, with lengths, Δl_f , corresponding to the lengths of the interacting region at the moment $t = t_h$, even if the final rapidity, y_f , was not yet achieved for this particular collision.⁴ On the other hand the time, t_h , cannot be longer than the time for which the simple analytical solution presented in the previous section is valid. I.e., $t_h \leq \text{Minimum}\{t_{form,i} + t_{over,i}\}$, where $t_{form,i}$ is a time of formation of the final streak for particular streak-streak collisions i : when the larger of two initial streak gets rapidity y_f (given by eq. (43) in Ref. [70]); $t_{over,i}$ is given by eq. (68). In this section we present all the results at $t_h = 5 \text{ fm}/c$, while for $\varepsilon_0 = 100 \text{ GeV}/nucl$, $b = 0.25 \cdot 2 R_{Au}$, $A = 0.08$ the maximal possible $t_h = \text{Minimum}\{t_{form,i} + t_{over,i}\} \approx 5.04 \text{ fm}/c$.

The reader may notice that all of the above discussion about final streaks is for the energy density distribution. What about the baryon charge distribution in the final streaks? Our knowledge here is very poor and, in principle, we are free to assume anything between two extreme cases: A) the complete transparency picture, where charges would remain at the ends of the final streak; this is the qualitative picture in Ref. [71]; B) homogeneous in baryon charge final streaks, the simplified situation discussed in Refs. [68–70]

First, we present the initial rapidities for final streaks for different x coordinates in the reaction plane – Fig. 10. Fig. 11 shows the energy density distribution in the reaction plane with non-expanding final streaks (Au+Au collision at $\varepsilon_0 = 65 \text{ GeV}/nucl$, $b = 0.25 \cdot 2 R_{Au}$, $A = 0.08$). Fig. 12 shows the energy density distribution in the reaction plane for the same collision, but with expanding streaks. The QGP forms a tilted disk for $b \neq 0$. Thus, the direction of fastest expansion, the same as the largest pressure gradient, will be in the reaction plane, but will deviate from both the beam axis and the usual transverse flow direction. So, the new flow component, called “antiflow” or “third flow component” (see section 2.5), appears in addition to the usual transverse flow component in the reaction plane (for non-expanding streaks this was shown in [78–80]). With increasing beam energy the usual transverse flow is getting weaker, while this new flow component is strengthened.

⁴ The calculations of the initial state presented in this section are done for colliding nuclei with a homogeneous density distribution. The modification is pretty straightforward - we can use the Wood-Saxon density distribution for the Au nucleus in our case. This will lead to the increasing of the density in the middle of the colliding nuclei, therefore the middle streaks will contain more partons, will generate a stronger field and, thus, will form the final streaks faster. While the peripheral streaks will contain less matter, therefore their dynamics, which is oversimplified, will have less influence on the final state.

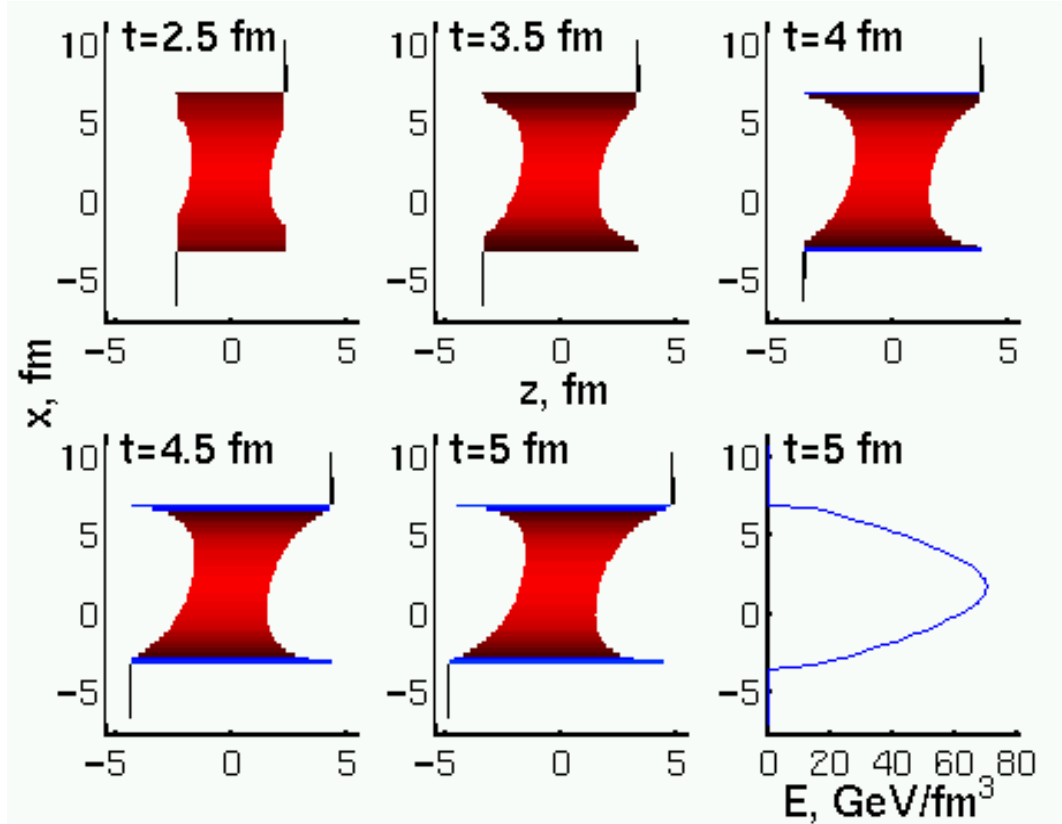


Fig. 11. Au+Au collision at $\varepsilon_0 = 65 \text{ GeV}/\text{nucl}$, $b = 0.25 \cdot 2 R_{Au}$, $A = 0.08$ (the parameter A was introduced in eq. (32)), $E = T^{00}$ is presented in the reaction plane as a function of x and z for different times in the laboratory frame. The final shape of the QGP volume is a tilted disk $\approx 45^\circ$, and the direction of the fastest expansion will deviate from both the beam axis and the usual transverse flow direction and will generate the third flow component [78–80]. Note that the initial state for hydro looks pretty much like the one discussed in the “firestreak” model (see Fig. 4), since the final streaks are moving with rapidities presented in Fig. 10. These calculations are done for the symmetrized $\tilde{T}^{\mu\nu}$ (see eq. 35), but the results do not differ too much from what is presented in Ref. [70].

More results for full RHIC energy ($\varepsilon_0 = 100 \text{ GeV}/\text{nucl}$) for different string tensions and impact parameters are presented in Figs. 13–14.

Note that the initial state with non-expanding streaks (Figs. 11) looks pretty much like the one discussed in “firestreak” model (see Fig. 4), since the final streaks are moving with rapidities presented in Fig. 10. If we let final streaks expand, this smooths over picture, but most of the matter, nevertheless, keeps similar energy density profile and velocity distributions.

From Figs. 11 and 13-14 we may see that for the central collisions at $\varepsilon_0 = 100 \text{ GeV}/\text{nucl}$ the maximum energy density $E = T^{00}$ reaches as high as $E_{max} \approx 100 \text{ GeV}/\text{fm}^3$. It seems to be larger than what one should expect from the Bjorken estimate (see section 2.3) - $e_0 = 4.3 \text{ GeV}/\text{fm}^3$ for

$\sqrt{s} = 130 A \text{ GeV}$ [75]. This is natural since our initial energy density distribution is much more peaked as a function of z than is the one obtained in the Bjorken picture (our energy density distribution is also peaked as a function of transverse coordinate (x, y) , but here the difference seems to be not that large, see for example [33]). One should, nevertheless, keep in mind that we have also a huge initial pressure, $P = c_0^2 e$, which will cause a fast hydrodynamical expansion, and thus, as discussed in section 2.3, will reduce $\left(\frac{dE_T}{dy}\right)_{y=0}$. This is a usual situation for hydrodynamical calculation, for example, in Ref. [33] $e_0 = 23 \text{ GeV}/fm^3$ has been used to reproduce the elliptic flow at RHIC for $\varepsilon_0 = 65 \text{ GeV}/nucl$, although the Bjorken initial geometry had been assumed.

In a recent work [77] another scenario of the creation of the third flow component based on the shadowing picture was proposed. The calculations were performed in the framework of QGSM. The shadowing effect manifests itself in the following way - hadrons emitted at small rapidities in the antiflow direction can propagate freely, while hadrons emitted in the normal directed flow direction still remain within the expanding subsystem of interacting particles. We would like to point out how one can distinguish this scenario from the one discussed above in this paper. The tilted initial state has the maximal effect for non-zero, but not very large, impact parameters, approximately up to $b = 0.5(R_A + R_B)$, i.e., in semicentral reactions. For semiperipheral and peripheral collisions our string rope tension, σ , would be small, and we would have to wait for a long time for the final streak formation, i.e., at the initial stages we would have one-dimensional Bjorken transparency. On the other hand, shadowing just becomes stronger with increasing impact parameter and gives the most drastic effect for semiperipheral and peripheral collisions.

4 Conclusions

A realistic and detailed description of an energetic heavy ion reaction requires a Multi Module Model, wherein the different stages of the reaction are each described with a suitable theoretical approach. The initial stages are the most problematic at RHIC energies. We tried to show that for the qualitative understanding of the basic features of the initial stages a phenomenological “firestreak” model can be used. For the detailed calculations of the initial state the Effective String Rope model has been developed. This model is based on earlier Coherent Yang-Mills field theoretical models and introduces an effective string tension based on Monte-Carlo string cascade and parton cascade model results. Contrary to earlier expectations based on standard string tensions of $1 \text{ GeV}/fm$, which lead to the Bjorken model type of initial state, the effective string tension introduced in our model for collisions of energetic massive heavy ions causes limited transparency. The increased string tension is a

consequence of collective effects related to QGP formation. These collective effects in central and semicentral collisions lead to an effective string tension of the order of $10 \text{ GeV}/fm$ and consequently cause much less transparency than earlier estimates. The resulting initial locally equilibrated state of matter in semicentral collisions takes a rather unusual form (see Figs. 11, 12, 13-14) and the resulting flow velocity field (see Fig. 10, 7 (D)) is in agreement with the “firestreak” phenomenological picture. Such an initial state will manifest itself by the asymmetry of the produced collective flow, even after the subsequent hydrodynamical expansion [78–80].

Acknowledgment

Two of us (V.K.M and D.D.S.) thank the support of the Bergen Computational Physics Laboratory in the framework of the European Community - Access to Research Infrastructure action of the Improving Human Potential Programme and the Humboldt Foundation.

A Initial conditions after string creation

Our conserved quantities are (36, 37)

$$Q^0 = \int \tilde{T}^{00} dV = \Delta x \Delta y \int \tilde{T}^{00} dz , \quad (\text{A.1})$$

$$Q^3 = \int \tilde{T}^{03} dV = \Delta x \Delta y \int \tilde{T}^{03} dz , \quad (\text{A.2})$$

where \tilde{T}^{00} and \tilde{T}^{03} are given by eq. (38). Before string creation the initial values of the modified energy-momentum tensor, $\tilde{T}^{\mu\nu}$, are

$$\tilde{T}_1^{00} = \tilde{T}_2^{00} = e_0 \cosh^2 y_0 = \left(\frac{\varepsilon_0}{m}\right)^2 n_0 m , \quad (\text{A.3})$$

$$\tilde{T}_2^{03} = -\tilde{T}_1^{03} = e_0 \tanh y_0 \cosh^2 y_0 = \left(\frac{\varepsilon_0}{m}\right)^2 n_0 m v_0 \quad (\text{A.4})$$

where m is the nucleon mass, ε_0 is the initial energy per nucleon, and we have used $\cosh^2 y_0 = \gamma_0^2 = \left(\frac{\varepsilon_0}{m}\right)^2$. $v_0 = \tanh y_0$ is the initial velocity, $v_0 = 1$ is a good approximation for ultra-relativistic heavy ion collisions. Thus,

$$Q^0 = \Delta x \Delta y \left(\frac{\varepsilon_0}{m}\right)^2 n_0 m (l_1 + l_2) , \quad (\text{A.5})$$

$$Q^3 = \Delta x \Delta y \left(\frac{\varepsilon_0}{m} \right)^2 n_0 m (l_2 - l_1) v_0 , \quad (\text{A.6})$$

where l_1 and l_2 are the initial lengths of streaks (see Fig. 5), Δx , Δy are the grid sizes in x and y directions. Thus the rapidity of CM frame is

$$\tanh y = \frac{Q^3}{Q^0} = \frac{v_0}{M} , \quad (\text{A.7})$$

where

$$M = \frac{l_2 + l_1}{l_2 - l_1} . \quad (\text{A.8})$$

After string creation –

$$\begin{aligned} \tilde{T}^{00} &= e_1 \cosh^2 y_1 + c_0^2 e_1 \sinh^2 y_1 + e_2 \cosh^2 y_2 + c_0^2 e_2 \sinh^2 y_2 \\ &+ \frac{1}{2} \sigma^2 + B - \frac{\sigma x^+}{2} n_0 e^{-y_0} e^{2y_1} - \frac{\sigma x^-}{2} n_0 e^{-y_0} e^{-2y_2} , \end{aligned} \quad (\text{A.9})$$

$$\begin{aligned} \tilde{T}^{03} &= e_1 (1 + c_0^2) \cosh y_1 \sinh y_1 + e_2 (1 + c_0^2) \cosh y_2 \sinh y_2 \\ &- \frac{\sigma x^+}{2} n_0 e^{-y_0} e^{2y_1} + \frac{\sigma x^-}{2} n_0 e^{-y_0} e^{-2y_2} , \end{aligned} \quad (\text{A.10})$$

At the point of complete penetration of streaks, $t = t_0 = (l_1 + l_2)/2$ (see Fig 5), we introduced energy densities $e_1(t_0)$ and $e_2(t_0)$. We assumed transparency, i.e., that complete penetration happened so fast, that the field itself that was created during this time did not have time to stop partons. So, the rapidities $y_{1(2)}(t_0) = -y_0(y_0)$ correspondingly, and the proper baryon densities did not change, and thus, the baryon current is conserved. Then the energy and momentum conservation laws can be written in the form:

$$\begin{aligned} \frac{Q^0}{\Delta x \Delta y} &= \left[(1 + c_0^2) \cosh^2 y_0 - c_0^2 \right] (e_1(t_0) l_1 + e_2(t_0) l_2) \\ &+ \left(\frac{\sigma^2}{2} + B \right) (l_1 + l_2) + \frac{\sigma n_0 e^{-y_0}}{4} (l_1^2 + l_2^2) , \end{aligned} \quad (\text{A.11})$$

$$\begin{aligned} \frac{Q^3}{\Delta x \Delta y} &= \left[(1 + c_0^2) \cosh^2 y_0 \right] (-e_1(t_0) l_1 + e_2(t_0) l_2) \\ &- \frac{\sigma n_0 e^{-y_0}}{4} (l_1^2 - l_2^2) . \end{aligned} \quad (\text{A.12})$$

We neglect c_0^2 next to $(1 + c_0^2) \cosh^2 y_0$ in eq. (A.11), then eqs. (A.11, A.12) may be solved

$$e_1(t_0) = \frac{n_0 m}{1+c_0^2} - \frac{\frac{\sigma^2}{2} + B}{\left(\frac{\varepsilon_0}{m}\right)^2 (1+c_0^2)} \frac{l_1+l_2}{2l_1} - \frac{\sigma n_0 e^{-y_0}}{4 \left(\frac{\varepsilon_0}{m}\right)^2 (1+c_0^2)} l_1, \quad (\text{A.13})$$

$$e_2(t_0) = \frac{n_0 m}{1+c_0^2} - \frac{\frac{\sigma^2}{2} + B}{\left(\frac{\varepsilon_0}{m}\right)^2 (1+c_0^2)} \frac{l_1+l_2}{2l_2} - \frac{\sigma n_0 e^{-y_0}}{4 \left(\frac{\varepsilon_0}{m}\right)^2 (1+c_0^2)} l_2. \quad (\text{A.14})$$

References

- [1] Josef Sollfrank *et al.*, Phys. Rev. C **55**, 392 (1997).
- [2] U. Ornik, M. Pluemer, B.R. Schlei, D. Strottman, R. M. Weiner Phys. Rev. C **54** 1381 (1996).
- [3] P.F. Kolb, J. Sollfrank, U. Heinz, Phys. Rev. C **62**, 054909 (2000).
- [4] P.F. Kolb, P.Huovinen, U. Heinz, H. Heiselberg, Phys. Lett **B500**, 232 (2001).
- [5] P. Huovinen, P.F. Kolb, U. Heinz, H. Heiselberg, Phys. Lett **B503**, 58 (2001).
- [6] D. Teaney, J. Lauret, and E.V. Shuryak, Phys. Rev. Lett. **86**, 4783 (2001).
- [7] D. Molnar and M. Gyulassy, Nucl. Phys. **A697** (2002) 495.
- [8] M. Bleicher and H. Stocker, Phys. Lett. **B526** 309 (2002).
- [9] Cs. Anderlik, Z.I. Lázár, V.K. Magas, L.P. Csernai, H. Stöcker and W. Greiner, Phys. Rev. C **59** 388 (1999).
- [10] Cs. Anderlik, L.P. Csernai, F. Grassi, W. Greiner, Y. Hama, T. Kodama, Zs. Lazar, V. Magas and H. Stöcker, Phys. Rev. C **59** 3309 (1999); Phys. Lett. **B459** 33 (1999).
- [11] V.K. Magas, Cs. Anderlik, L.P. Csernai, F. Grassi, W. Greiner, Y. Hama, T. Kodama, Zs. Lázár and H. Stöcker, Heavy Ion Phys. **9** 193 (1999); Nucl. Phys. **A661** 596 (1999).
- [12] A. Keränen, J. Manninen, L.P. Csernai and V.K. Magas, nucl-th/0205019.
- [13] S. Bass, A. Dumitru, Phys. Rev. C **61** 064909 (2000).
- [14] D. Teaney, J. Lauret, E.V. Shuryak, nucl-th/0110037.
- [15] A.A. Amsden, A.S. Goldhaber, F.H. Harlow and J.R. Nix, Phys. Rev. C **17** 2080 (1978).
- [16] L.P. Csernai, I. Lovas, J. Maruhn, A. Rosenhauer, J. Zimanyi, W. Greiner, Phys. Rev. C **26** 149 (1982).

- [17] J. Brachmann, S. Soff, A. Dumitru, H. Stöcker, J.A. Maruhn, W. Greiner, D.H. Rischke, L. Bravina, Phys. Rev. C **61** 024909 (2000).
- [18] S.A. Bass *et al.*, Prog. Part. Nucl. Phys. **41** 225 (1998).
- [19] D. Molnar, M. Gyulassy, Phys. Rev. C **62** 054907 (2000).
- [20] D. Molnar, M. Gyulassy, in *Proceedings of the 30th International Symposium on Multiparticle Dynamics (ISMD 2000), Tihany, Lake Balaton, Hungary, 9-15 Oct 2000*, edited by T. Csörgö, S. Hegyi and W. Kittel (World Scientific, Singapore, 2001), p. 552; Nucl. Phys. **A698** 379 (2002).
- [21] EM Collab., J. Ashman *et al.*, Phys. Lett. **B202** 603 (1988); EM Collab., M. Arneodo *et al.*, Phys. Lett. **B211** 493 (1988).
- [22] M. Gyulassy, Xin-Nian Wang, Comput. Phys. Commun. **83** 307 (1994).
- [23] V. Emelyanov, A. Khodinov, S.R. Klein, R. Vogt, Phys. Rev. C **61** 044904 (2000).
- [24] M. Gorenstein (private communication).
- [25] L. McLerran, R. Venugopalan, Phys. Rev. D **49** 2233 (1994); **49** 3352 (1994); A. Krasnitz, R. Venugopalan, Phys. Rev. Lett. **84** 4309 (2000); hep-ph/0004116.
- [26] J.P. Blaizot, A.H. Mueller, Nucl. Phys. **B289** 847 (1987); A.H. Mueller, Nucl. Phys. **B572** 227 (2000).
- [27] K.J. Eskola, K. Kajantie, P.V. Ruuskanen, K. Tuominen, Nucl. Phys. **B570** 379 (2000).
- [28] K.J. Eskola, K. Tuominen, Phys. Lett. **B489** 329 (2000); Phys. Rev. D **63** 114006 (2001).
- [29] K.J. Eskola, K. Kajantie, K. Tuominen, Phys. Lett. **B497** 39 (2001).
- [30] K.J. Eskola, P.V. Ruuskanen, S.S. Rasanen, K. Tuominen, Nucl. Phys. **A696** 715 (2001).
- [31] J.D. Bjorken, Phys. Rev. D **27** 140 (1983).
- [32] K. Kajantie, R. Raitio, V. Ruuskanen, Nucl. Phys. **B222** 1304 (1986).
- [33] P.F. Kolb, U. Heinz, P. Huovinen, K.J. Eskola, K. Tuominen, Nucl. Phys. **A696** 197 (2001).
- [34] M. Gyulassy, L.P. Csernai, Nucl. Phys. **A460** 723 (1986).
- [35] P. Steinberg, Nucl. Phys. **A698** 193 (2002); R. Snellings, A. Drees, talks at the Quark Matter 2001, Stony Brook, NY, USA, January 15-20, 2001.
- [36] STAR Collaboration, Phys. Rev. Lett. **87** 112303 (2001).
- [37] S. Voloshin and Y. Zhang, Z. Phys. C **70** 665 (1996).
- [38] A.M. Poskanzer and S.A. Voloshin, Phys. Rev. C **58** 1671 (1998).

- [39] A. Dumitru, M. Gyulassy, Phys. Lett. **B494** 215 (2000).
- [40] PHENIX Collaboration, Nucl. Phys. **A698** 559 (2002); PHOBOS Collaboration, Nucl. Phys. **A698** 564 (2002); STAR Collaboration, Phys. Rev. Lett. **86** 401 (2001); Phys. Rev. Lett. **87** 182301 (2001).
- [41] F. Videbaek, talk at the Quark Matter 2001, Stony Brook, NY, USA, January 15-20, 2001.
- [42] C. Adler, *et al.*, (STAR Collaboration), Phys. Rev. Lett. 4778 **86** (2001).
- [43] L. Bravina, L.P. Csernai, P. Lévai, and D. Strottman, - Proc. of the Int. Conf. Heavy-Ion Physics at the AGS: HIPAGS '93, Jan. 13-15, 1993, (MIT, Boston, Massachusetts, USA, 1993) p. 333.
- [44] L.P. Csernai, D. Röhrich, Phys. Lett. **B458** 454 (1999).
- [45] A. K. Holme, E. F. Staubo, L.P. Csernai, E. Osnes, D. Strottman, Phys. Rev. D **40** 3735 (1989).
- [46] N. S. Amelin, E.F. Staubo, L.P. Csernai, V.D. Toneev, K.K. Gudima and D.D. Strottman, Phys. Rev. Lett. **67** 1523 (1991).
- [47] L. Bravina, L.P. Csernai, P. Lévai and D. Strottman, Phys. Rev. C **50** 2161 (1994).
- [48] D.H. Rischke, Y. Pürsün, J.A. Maruhn, H. Stöcker and W. Greiner, Heavy Ion Phys. **1** 309 (1995).
- [49] C.M. Hung and E.V. Shuryak, Phys. Rev. Lett. **75** 4003 (1995).
- [50] J. Brachmann, A. Dumitru, J.A. Maruhn, H. Stöcker, W. Greiner and D. Rischke, Nucl. Phys. **A619** 391 (1997).
- [51] H. Liu, S. Panitkin and N. Xu, Phys. Rev. C **59** 348 (1999).
- [52] L. Bravina, Phys. Lett. **B344** 49 (1995).
- [53] J. Barette *et al.* (E814 Collaboration), Phys. Rev. Lett. **73** 2532 (1994); Phys. Lett. **B351** 93 (1995).
- [54] J. Barette *et al.* (E877 Collaboration), Phys. Rev. C **55** 1420 (1997); Phys. Rev. C **56** 3254 (1997).
- [55] N.N. Ajitanand *et al.* (E895 Collaboration), Nucl. Phys. **A638** 415 (1997).
- [56] H. Appelshäuser *et al.* (NA49 Collaboration), Nucl. Phys. **A638** 463 (1998); Phys. Rev. Lett. **80** 4136 (1998).
- [57] M. Kurata *et al.* (WA98 Collaboration); S. Nishimura *et al.* talks given at the 3rd International Conference on Physics and Astrophysics of Quark Gluon Plasma (ICPAQGP 97), Jaipur, India; M.M. Aggrawal *et al.* (WA98 Collaboration), Nucl. Phys. **A638** 459 (1998); nucl-ex/9807004.

- [58] A.M. Poskanzer and S.A. Voloshin, Phys. Rev. C **58** 1671 (1998).
- [59] H. Sorge, Phys. Rev. Lett. **82** 2048 (1999).
- [60] D. Myers, Nucl. Phys. **A296** 177 (1978).
- [61] J. Gosset, J.I. Kapusta and G.D. Westfall, Phys. Rev. C **18** 844 (1978).
- [62] T.S. Biró, H.B. Nielsen, J. Knoll, Nucl. Phys. **B245** 449 (1984).
- [63] H. Sorge, Phys. Rev. C **52** 3291 (1995).
- [64] K. Werner, J. Aichelin, Phys. Rev. Lett. **76** 1027 (1996).
- [65] N.S. Amelin, M.A. Braun, C. Pajares, Phys. Lett. **B306** 312 (1993), Z. Phys. C **63** 507 (1994).
- [66] N. S. Amelin, E.F. Staubo, L.P. Csernai, V.D. Toneev, K.K. Gudima and D.D. Strottman, Phys. Lett. **B261** 352 (1991).
- [67] N.S. Amelin, L.P. Csernai, E.F. Staubo, and D. Strottman, Nucl. Phys. **A544** 463 (1992).
- [68] V.K. Magas, L.P. Csernai, D.D. Strottman, in Proceedings of the New Trends in High-Energy Physics, Yalta (Crimea), Ukraine, May 27 - June 4, 2000, edited by P.N. Bogolyubov and L.L. Jenkovszky (Bogolyubov Institute for Theoretical Physics, Kiev, 2000), p. 93, nucl-th/0009049; in Proceedings of the ISMD 2000 - XXXth International Symposium on Multiparticle Dynamics, Tihany, Lake Balaton, Hungary, October 9-15, 2000, edited by T. Csörgo and S. Hegyi and W. Kittel (World Scientific) p. 523, hep-ph/0101125.
- [69] L.P. Csernai, Cs. Anderlik, V.K. Magas, in Proceedings of the Symposium on Fundamental Issues in Elementary Matter, Bad Honnef, Germany, September 25-29, 2000, edited by W. Greiner (EP Systema Bt., Debrecen, 2001), p. 77, nucl-th/0010023.
- [70] V. Magas, L.P. Csernai, D. Strottman, Phys. Rev. C **64** 014901 (2001).
- [71] I.N. Mishustin, J.I. Kapusta, Phys. Rev. Lett. **88** (2002) 112501.
- [72] L.D. Landau, E.M. Lifshits, Course of Theoretical Physics, Vol. 2, *Field theory*.
- [73] D. Kharzeev and E. Levin, Phys. Lett. **B523** 79 (2001).
- [74] K. Kajantie, T. Matsui, Phys. Lett. **B164** 373 (1985).
- [75] A. Milov, talk at the Quark Matter 2001, Stony Brook, NY, USA, January 15-20, 2001.
- [76] R.J.M. Snellings, H. Sorge, S.A. Voloshin, F.Q. Wang, N. Xu, Phys. Rev. Lett. **84** 2803 (2000).
- [77] E. E. Zabrodin, C. Fuchs, L. V. Bravina, A. Faessler, *Phys. Rev. C* **63** (2001) 034902.

- [78] V.K. Magas, PhD Thesis, Aug 2001, University of Bergen, Norway.
- [79] V.K. Magas, L.P. Csernai and D. Strottman, hep-ph/0110347, in Proceedings of the New Trend in High-Energy Physics, Yalta, Ukraine, September 22-29, 2001 - in press.
- [80] L.P. Csernai, Cs. Anderlik, V.K. Magas and D. Strottman, in Proceedings of the International Workshop On The Physics of The Quark Gluon Plasma, September 4-7, 2001, Palaiseau, Paris, France - in press, <http://polywww.in2p3.fr/CIPPQG/trans/Csernai.ppt>
- [81] D. Rischke, S. Bernard, J.A. Maruhn, Nucl. Phys. **A595** 346 (1995).
- [82] L.D. Landau, E.M. Lifshitz, *Fluid mechanics* (Pergamon, New York, 1959).
- [83] R. Courant, K.O. Friedrichs, *Supersonic flow and shock waves* (Springer, New York, 1985).
- [84] T. Hirano, Phys. Rev. C **65** 011901 (2002).

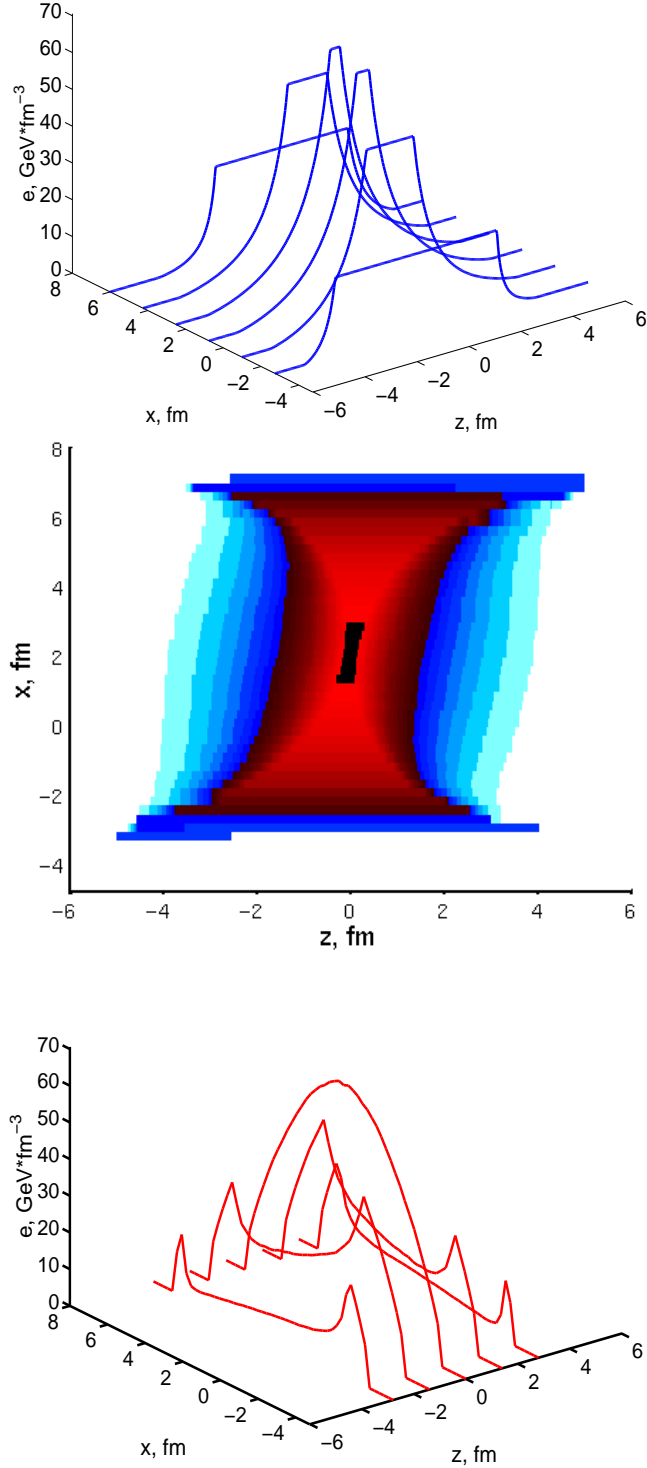


Fig. 12. Simulation of the same collisions as in Fig. 11 (Au+Au, $\varepsilon_0 = 65 \text{ GeV}/\text{nucl}$, $b = 0.25 \cdot 2 R_{Au}$, $A = 0.08$), but with expanding final streaks. The middle subplot presents $e(x, z)$ in the reaction plane for $t_h = 5 \text{ fm}/c$. The upper subplot shows the e profiles for different $x = \text{const}$. We can clearly see three regions - two of forward and backward rarefaction and middle where the initial energy density, e_f (eq. (42)), is still preserved. The lower subplot shows the e profiles for different $z = \text{const}$.

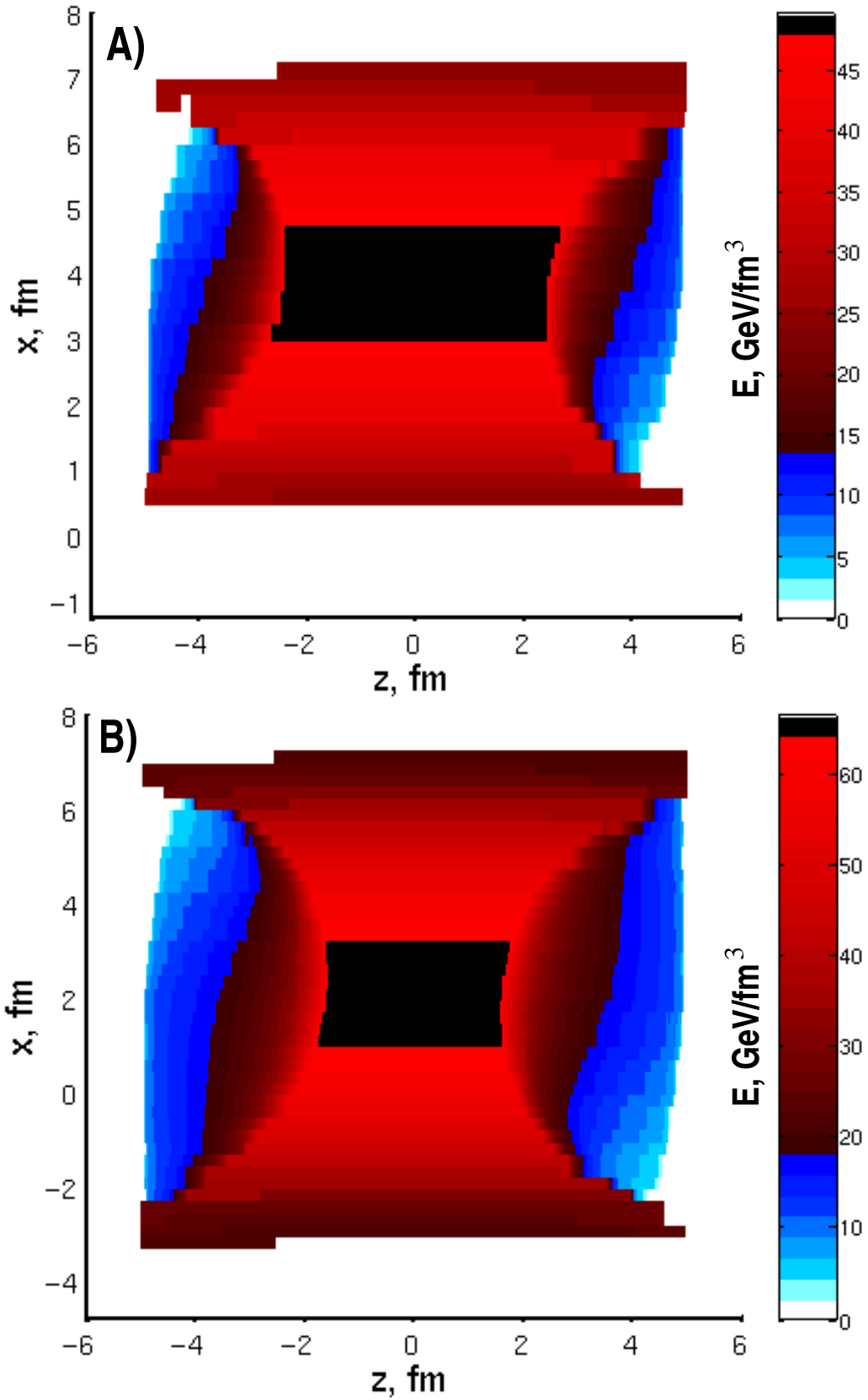


Fig. 13. Au+Au collision at $\varepsilon_0 = 100 \text{ GeV}/\text{nucl}$, $A = 0.065$, $E = T^{00}$ is presented in the reaction plane as a function of x and z for $t_h = 5 \text{ fm}/c$. Subplot A) ($b = 0.5 \cdot 2 R_{Au}$), subplot B) ($b = 0.25 \cdot 2 R_{Au}$). The QGP volume has a shape of a tilted disk and may produce a third flow component.

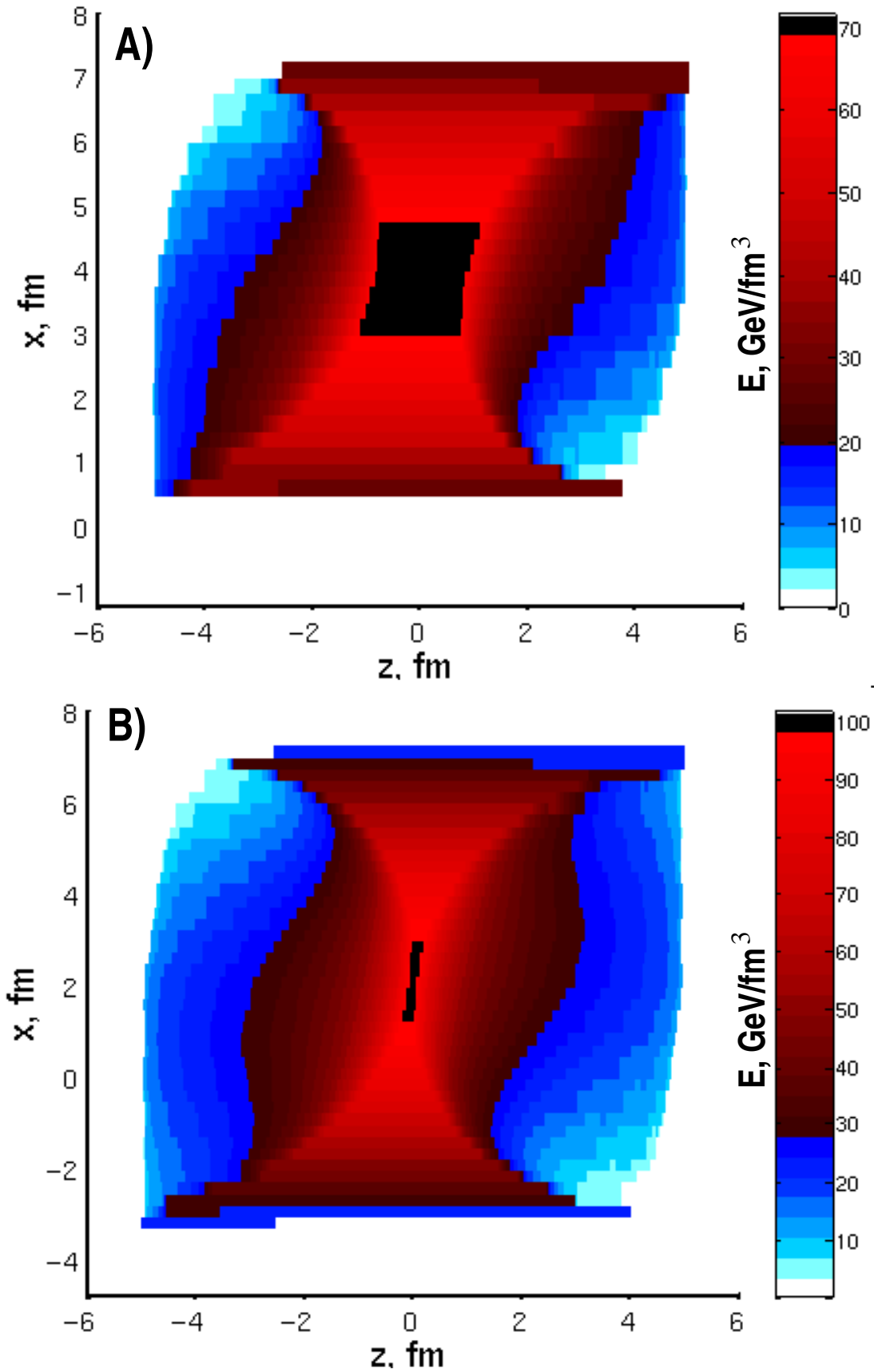


Fig. 14. The same as Fig. 13, but for $A = 0.08$. We see that due to a larger string tension the energy density is much larger.